DEVELOPMENT OF A STRAIN GAGE SIGNAL ANALYSIS TECHNIQUE TO DETERMINE TIME OF RIB FRACTURE IN THORACIC IMPACTS

Undergraduate Honors Thesis

Presented in Partial Fulfillment of the Requirements for

Graduation with Distinction

at The Ohio State University

By

Anthony Vergis

The Ohio State University

2011

Defense Committee:

Professor John Bolte, Adviser

Instructor Amanda Agnew

Dr. Richard Hughes

ABSTRACT

In 2010, 32,788 fatalities occurred due to automobile accidents, with a large portion of fatalities resulting from thoracic injuries. Data gathered from research on post mortem human surrogates (PMHS) can be used to improve the biofidelity of crash test dummies, a tool used to increase the safety of today's automobiles. The Injury Biomechanics Research Laboratory (IBRL) at The Ohio State University has conducted 13 PMHS tests to determine the response of the body to thoracic impacts. Strain gauges were attached to ribs to measure strain and predict the time of fracture of the ribs during the impact. However, upon initial inspection, the strain signals were not a reliable predictor of time of fracture. The purpose of this study was to analyze the strain gauge signals from previous tests to determine a quantitative measure that would signal if a fracture occurred or not. In this study, signals were compared to autopsy reports, which revealed the locations of actual fractures on the ribs. Single rib fracture studies were also completed, where ribs with strain gauges were broken ex vivo under the view of a high speed camera. From these tests, the strain gauge signal can be directly compared to the time of fracture, because the initiation of the fractures is evident on the video. Results from these tests and analysis of prior data show that there is correlation between the slope and strain drop-off in the signals and the time of rib fracture in the PMHS. The resulting quantitative analysis of the strain signals can be used to predict time of failure of ribs in past and future tests so proper injury predicting criteria of the thorax can be determined and used to improve the biofidelity of crash test dummies.

Dedicated to my mother for continually supporting me through my college education and giving me the occasional wakeup call so I never missed an exam

Acknowledgements:

I would first like to thank my advisor, Dr. John H. Bolte IV for his continued help with supporting my research, and helping me with all my questions throughout the years. I would also like to support Amanda Agnew and Yun-Seok Kang for providing me direction and helping to mentor me through the research process. I would also like to thank Dr. Hughes for reviewing my thesis and helping me complete this research in physics with an engineering laboratory. I would next like to thank Rod Herriott, Kevin Moorhouse, Heather Rhule, and all other employees at NHTSA VRTC and TRC who have helped to support the project that I have been completing. Finally, I would like to thank Julie Bing, Hannah Gustafson, Kyle Icke, Matt Kremer, Matt Long, Austin Meek, Brian Suntay, and all other people involved with the Injury Biomechanics Research Lab at The Ohio State University for helping to complete tests and answering questions for me along the way.

Table of Contents

List of Tables

List of Figures

Chapter 1: Introduction

In 2010, 32,788 fatalities occurred due to automobile accidents, with a large portion of fatalities resulting from thoracic [9]. Two factors that contribute to thoracic injury fatalities are pneumothorax and flail chest [2]. Both of these can be caused by damage to the bony rib cage. Flail chest especially is caused by multiple fractures in ribs. Due to this knowledge, it is becoming increasingly more important to study the dynamics of the thorax in a collision situation so that restraints can be developed that will prevent these life threatening thoracic injuries. Much of the testing is performed on Anthropomorphic Test Devices (ATDs).

Anthropomorphic Test Devices, which are commonly referred to as "Crash Dummies," are used in automotive safety research to predict responses of the human body during automobile collisions. These ATDs contain sensors that can measure forces, compressions, and angular rotations at multiple points throughout the ATD. However, it is not possible to know what the injury thresholds are for humans solely based on those data. Therefore post mortem human surrogate (PMHS) testing is performed to gain the response of the human body to different injurious impact events. These PMHS are obtained through willed body and body donor programs at various universities and hospitals. After being tested to make sure that a PMHS is safe and is representative of the population, it can be used in testing to determine the injury thresholds and dynamic response of the body to an impact. Long et al at The Ohio State University Injury Biomechanics Research Lab (IBRL) have been comparing the response of a PMHS between lateral and oblique impacts with a pneumatic ram [8].

A secondary study of the test is to determine the time of rib fracture during the impact. This is important because it can reveal the force and compression of the chest at the time that the rib failed so that the best predictors of injury during an impact can be developed. In order to determine the time of rib fractures, Vishay strain gages were applied to the ribs, and the strain was measured throughout various thoracic impacts. However, throughout these tests, it was not always easy to predict the time of fracture from the signal. Having the autopsy report helped to determine the presence of a fracture, but the signals were difficult to use qualitatively. Because it is difficult to obtain a PMHS, The Ohio State Injury Biomechanics Research Lab has started testing multiple times on a subject. However, multiple impacts cannot be completed if a rib has fractured. In the scenario of multiple tests, an autopsy cannot be performed in between the two tests, because it will damage the PMHS. Therefore, reliable strain gage signals are needed to determine whether or not a fracture occurred so testing can either continue or cease. The goal of this study is to develop a quantitative method to predict the likelihood of a rib fracture based on the strain gage signal and to compare results with results from *ex vivo* human rib testing to strengthen the conclusions about rib fractures in thoracic impact tests. This will be performed by completing the following objectives. The objectives of this study are as follows:

- Analyze strain gage data from the first 13 thoracic tests to determine a quantitative method to predict whether or not a rib fractured during the thoracic impact test before conducting an autopsy
- Analyze results from 4 *ex vivo* rib fracture pendulum tests to compare the signals from the thoracic data to signals where the fracture is visible and unobstructed
- Compare a recent thoracic test which used the new Vishay Strain Gages without exposed leads

- Use data from all tests to support the quantitative method developed for the thoracic data

Chapter 2: Background

This chapter will discuss the gross anatomy and related clinical knowledge about the thorax and ribs. It will also discuss strain and the strain gage.

2.1 Thorax Anatomy

The human thorax is the region of the human body most notable for containing the heart and lungs. It is bordered laterally on both the right and left side by the upper limbs. It is bordered superiorly by the neck and inferiorly by the diaphragm, which is a muscle separating the thorax from the abdomen. Figure 2.1 depicts the thorax deep to the thoracic wall. The thorax contains some of the most vital organs in the human body. The lungs are located laterally in Figure 2.1, and they are responsible for the exchange of oxygen and carbon dioxide in the blood stream as a person breathes. The heart is located in the pericardial cavity. It is responsible for transporting blood throughout the body. The arteries associated with the heart transport oxygenated blood throughout the body, and the veins transport deoxygenated blood back to the heart, with the exception of the pulmonary artery and vein. The pulmonary artery transports deoxygenated blood from the heart to the lungs, and the pulmonary veins transport oxygenated blood from the lungs to the heart. Also found deep to the thoracic wall are the esophagus and trachea. The trachea is anterior to the esophagus and transports air to and from the lungs, and the esophagus transports food to the stomach in the abdominal cavity as part of the digestive system.

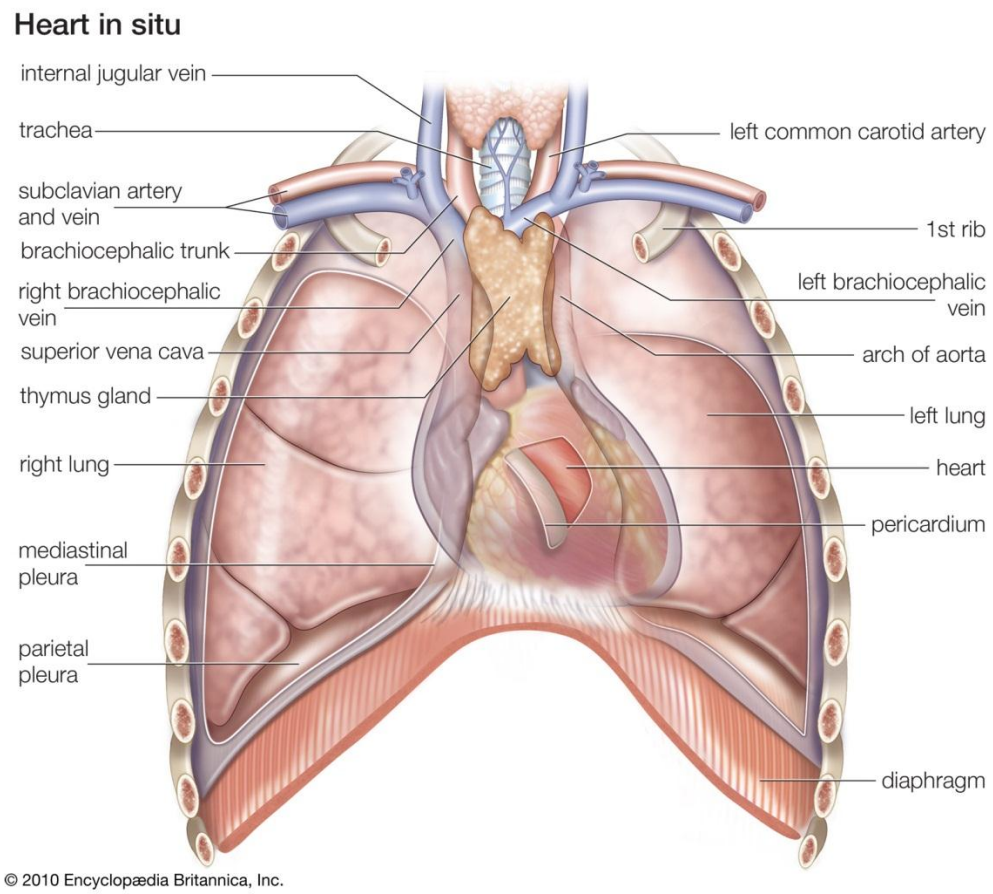

Figure 2.1: Thoracic Cavity [7]

The thoracic wall is depicted in Figure 2.2 and consists of the bony thorax. The bony thorax consists of 12 thoracic vertebrae as the posterior portion of the thoracic wall. Articulating with the vertebrae are 12 ribs, which form the oblique portion of the thoracic wall. Ribs 1-7, which are the 7 most superior ribs, are true ribs, ribs 8-10 are false ribs, and ribs 11 and 12 are floating ribs. The coastal cartilage, a type of hyaline cartilage articulates ribs 1-10 with the sternum in the anterior portion of the thorax. True ribs have costal cartilage that directly articulates with the sternum. False ribs have coastal cartilage that articulates with the coastal

cartilage of rib 7 to connect to the sternum. The floating ribs do not have coastal cartilage attached to them. The sternum consists of the manubrium superiorly, the sternal body medially, and the xiphoid process inferiorly. In the intercostal spaces, the spaces between the ribs lay muscles, arteries, veins, and nerves. The muscles that are involved in exhalation, the depression of the rib cage, are the internal intercostal muscles, the transverse thoracis muscles, and the serratus posterior inferior muscle. The muscles that are involved in inhalation, the elevation of the rib cage are the scalene muscles, external intercostal muscles and the serratus posterior superior muscle.

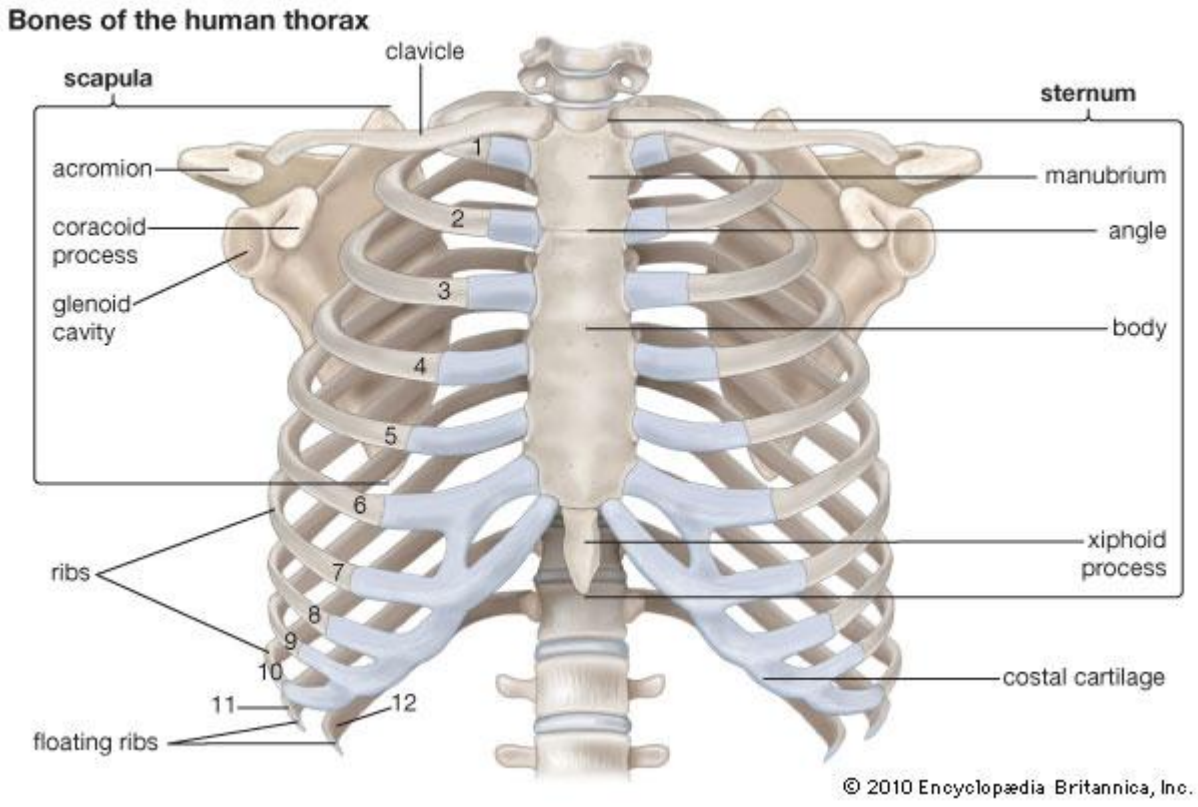

Figure 2.2: Bony Thorax [7]

As seen in Figure 2.3, each rib contains multiple distinctions. The head of the rib is the portion of the rib closest to the vertebrae. The neck is the flattened portion adjacent and lateral to

the head. The eminence lateral to the neck is the tubercle of the rib. The tubercle of the rib articulates with the vertebra through ligaments. Lateral and anterior to the tubercle is the costal angle, where the greatest curvature of the rib occurs. The body makes up the rest of the rib. Also included in the external structure of the rib is the costal groove, which is an elevated, flattened portion of the rib that runs along the inferior border of the rib. The superficial surface of the rib can also be called the cutaneous surface, and the deep surface can be called the pleural surface, since this portion rests against the lungs. Like all bones, the external surface, the cortical bone, is much harder and more solid than the inner bone. This trabecular bone is a meshwork material of bony matter and is less dense than cortical bone.

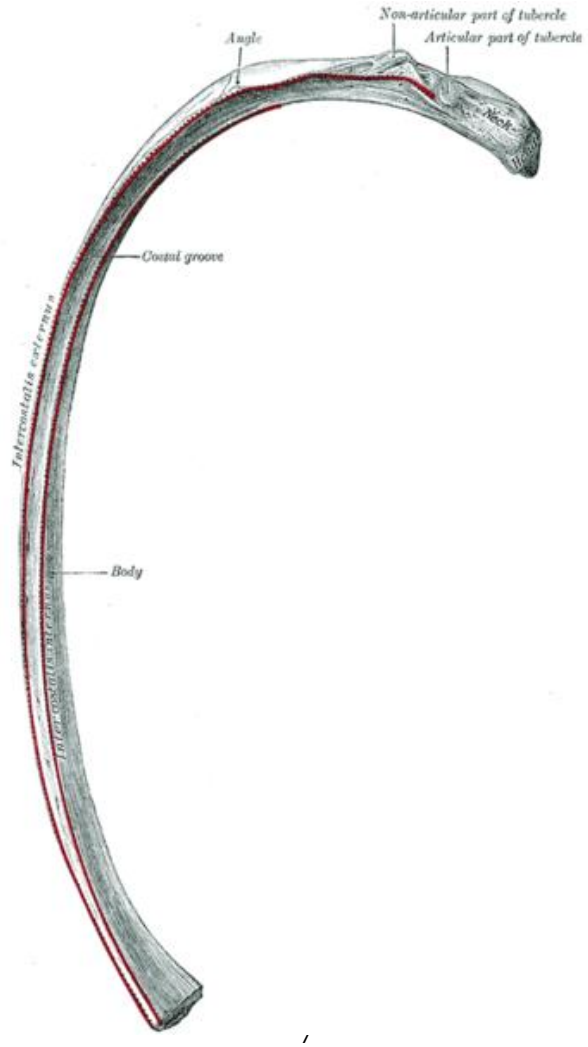

Figure 2.3: Inferior View: Human Rib [6]

2.2 Clinical Significance

Fractured ribs can be a problem for numerous reasons in trauma situations. One of the most prevalent problems caused by fractured ribs is flail chest, defined by multiple fractures in the rib cage, Flail chest is a condition where a person cannot breathe as easily as normal. One reason for this is because the thoracic wall does not contract and relax properly while breathing. However, it is not this breathing deficiency that generally causes fatalities in people who suffer flail chest. It is usually the pulmonary contusion that occurs along with the flail chest that causes enough structural damage to the lungs to increase the risk of fatal injuries. Autopsy confirmation of deaths occurring directly because of flail chest is usually difficult because a thoracic injury that fractures ribs is usually accompanied by other severe injuries. Borman et al showed that there is an increased mortality rate when flail chest accompanies other extrathoracic injuries. When a thoracic trauma fatality is related to complications resulting from flail chest, the death usually happens within 24 hours. Fatalities involving flail chest are also more likely to occur in elderly people. With current medical procedures, flail chest can be treated if it can be addressed before death [2].

2.3 Strain and the Strain Gauge:

Strain can be defined as a measurement of deformation of a material. At a rest, there is zero strain on an object. However, when a force is applied to an object and deformation occurs, strain builds up in the object. Stress is the specific acting power that causes strain. Stress is measured as a force applied over a given area and has the same units as pressure (N/m^2). A stress on an object causes a strain in the object, which is the resulting deformation. The strain can be measured as the change in length divided by the original length of the material. This makes the strain a unitless measure. A derived unit, strain, can be referred to as a strain of 1. However, most measurements of strain are taken in micro-strain, because deformations are usually much smaller. A micro strain is the strain multiplied by 10^6. Stress and strain can be related by Young's modulus, which is seen in equation 1 below.

1. $E = \text{stress}/\text{strain}$ (2.1)
2. $F = (E A_0 \Delta L)/L_0$ (2.2)

where F is the force applied, E is Young's modulus, A_0 is the original cross sectional area, ΔL is the change in length and L_0 is the original length

In a material, strain continues to build until the material fails. In this case, the strain decreases. If the force stops being applied, it will return to its normal zero value. The strain decreased because of either a break of a structural change in the material. In human ribs, the rib will fracture when enough strain is placed on it.

2.4 The Strain Gage

In general, a strain gage is a sensor that can determine the strain placed on an object that it is in direct contact with. On the face of the gage that is attached to the rib, there is a coil of a conductor. As electrical current flows through the conductor, the resistance can be measured. When strain occurs, the face of the strain gage changes shape, and a reduction or increase in the resistance of the coiled conductor ensues. Tension placed on the gage increases the resistance, and compression on the gage reduces the resistance. Figure 2.4 demonstrates the coils in the gage. As the current flows through the wire, the changes in resistance can be indirectly measured, and after a conversion factor is applied, the strain can be determined from this change in resistance [10].

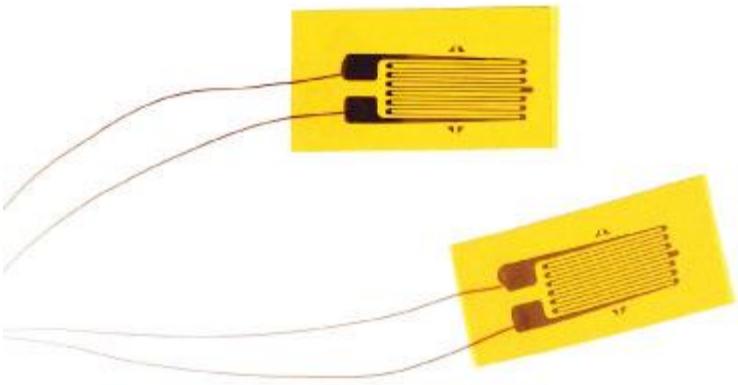

Figure 2.4: Coil Patterns on Strain Gages [10].

Chapter 3: Literature Review

There have been multiple studies analyzing rib fracture testing in impact studies. These tests have used multiple different application methods, gained multiple results, and have used different instruments to determine fracture timing. This study has been done in conjunction with results that were gained during a study completed by Matt Long at The Ohio State University Injury Biomechanics Lab. Concurrently a study was conducted at the Virginia Tech-Wake Forest Center for Injury Biomechanics that also used strain gages in a thoracic study to determine time of fracture. Another study has conducted rib fracture time analysis with piezoelectric transducers (PZTs). Research has also been done on single rib tests, showing properties of the human ribs and fracture patterns.

Much of this study has been done in parallel with the thoracic testing that was performed by Long et al. Long et al performed 9 PMHS tests of the thorax, all of which were included in the results of this study. In this study, the method for determining the time of fracture was to use the autopsy to determine how many fractures occurred at each rib. The next step was to qualitatively look at the strain gage signal to determine a sudden value change in the data. No comparison was made between regression slopes or maximum strain values and fracture, but fracture time estimates could still be determined because it was already known whether or not a fracture event was present in the signal because of autopsy reports. The point of fracture was defined as the point before a large drop-off in strain [8].

Duma et al also tested for rib fracture times with strain gages in thoracic impacts. In 2003, Duma et al performed a dynamic belt loading on the thorax of two PMHS. 47 strain gages were used on each subject's ribs. In this testing the skin was removed from the thorax and the strain gages were applied to each rib after this was completed. Gages were adhered along the axis of the rib and were relieved of tension in the wiring through wire ties around the rib as seen in Figure 3.1 [3,4].

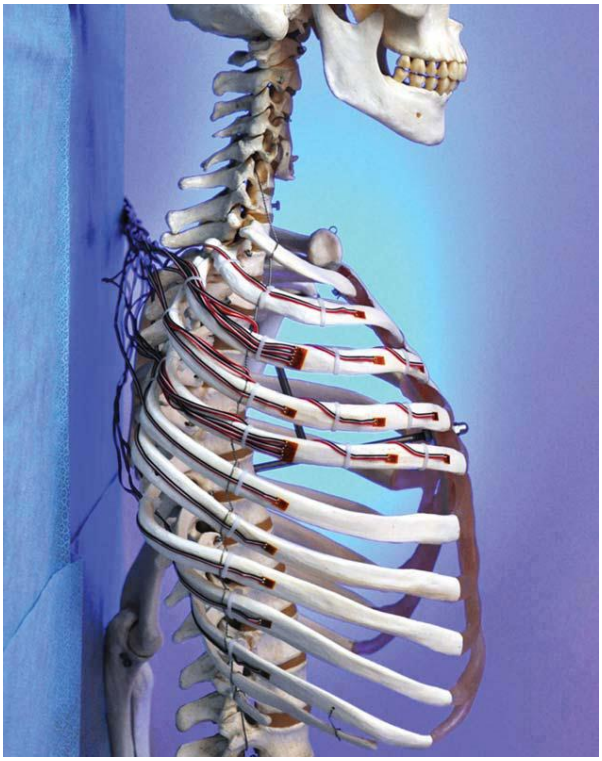

Figure 3.1: Duma et al Strain Gage Placement [4]

This figure shows the placement of the gages on the ribs, which was possible because the skin and subcutaneous tissue was removed from the thorax in one cut. The other major difference between the application of strain gages between the testing of Long et al and of Duma et al was

that Duma et al used an acidic solution to etch into the rib after clearing the surface and then neutralizing it with a basic solution. After obtaining results, multiple measurements were recorded. Maximum strain, time of maximum strain, and the strain rate were all recorded. The definition of the strain rate in this testing was determined by using the portion of the strain graph during loading that fit a linear regression best. This analysis showed a wide range of values between both the maximum strain and the strain rate. The signals after the peak were left out in case the strain gage broke or was detached from the rib after the rib fracture. The final determination of fracture was still found qualitatively as a "sudden drop in strain" signal [3,4].

Trosseille et al also looked at the strain and strain rate in tests where strain gages were applied to ribs during thoracic impacts. Maximum absolute strain and maximum absolute strain rate were compared to one another. In this study, it was determined that the fractured ribs had generally larger maximum absolute strains and maximum absolute strain rates than the non-fractured ribs. This test used filtered results, which allowed the maximum absolute strain rate to be studied. This study used up to 98 strain gages on each of 8 PMHS. A set strain rate for fracture prediction was not defined [11].

Because of time, cost, and sensitivity concerns with strain gages, Gabrielli et al set out to create a new method to determine rib fracture times that did not have the same problems the strain gage technology has. This study set out to use a different instrument for rib fracture time determination, piezoelectric transducers (PZTs). PZTs are instruments that convert deformations into a measurable change in voltage by detecting mechanical vibrations. Gabrielli et al were able to determine a range of frequency signals for the mechanical vibrations that correlated to fractures on both the instrumented rib and an adjacent rib. This study still has many limitations though. The signals cannot tell which adjacent rib the fracture is located on, so PZTs would have

to be used on most or all ribs still to determine a fracture times with confidence. While this new instrumentation has promise for the future to alleviate difficulty understanding strain gage data, this new technique still has limitations which must be minimized [5].

Chapter 4: Methods

This chapter contains four sections. The first section is a brief overview of the overall thoracic tests in which the strain gages were used. The second section contains a more in depth look at the application of strain gages throughout testing. The third section details the *ex vivo* rib tests. Finally, the fourth section details data analysis.

4.1 Original Thoracic Impact Summary

Fourteen thoracic impact trials were conducted in which strain gages were used to determine the time of rib fracture. For each of the tests, after a subject was received, the subject was first anzlyzed to make sure it was a usable subject, because every PMHS had to be representative of the human population. Blood tests or medical histories were analyzed to ensure the safety of lab personnel. A Body Mass Index (BMI) test was completed by utilizing the weight and height of the PMHS. Subjects were only accepted if they fell within the normal or overweight range in the BMI logarithm. After this was performed, a bone mineral density (BMD) scan was performed on each PMHS. This test was performed to ensure that subjects were not osteoporotic, because osteoporotic bones are much weaker than healthy bones and would not be representative of the population. Other abnormalities in the subjects were also recorded so that if any abnormal results occurred because of them, they would be noted as a potential reason.

After the subject was cleaned and prepared, it was instrumented. Angular Rate Sensors and Accelerometers were attached to subjects. They were placed on 3aω blocks (Figure 4.1).

Each of these blocks contained three accelerometers and three angular rate sensors. They were placed on the sternum and the T4 vertebra to measure the accelerations and angular motions of the subject during the impact.

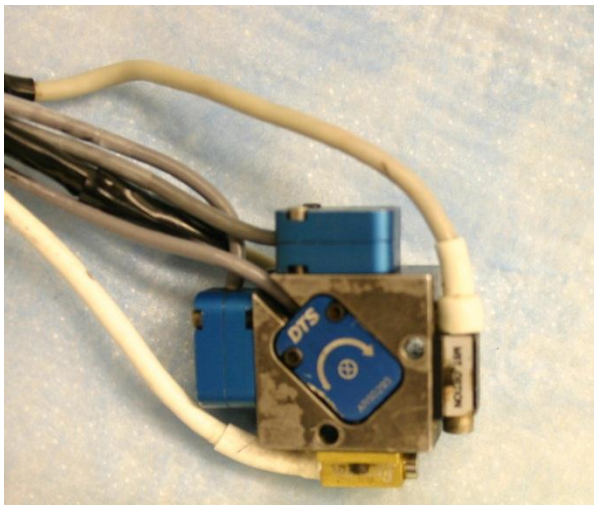

Figure 4.1: 3aω block

After the subject was instrumented, it underwent a CT scan to determine any pre-impact injuries and to use as an injury comparison to a post-test CT scan. After this, the subject was placed on a table in a seated position. The subject was positioned into the proper position, and then coordinates of the subject were measured with a FARO device. High Speed Cameras were setup before the test to capture the impact. After all was set up, the PMHS was impacted either laterally or obliquely in the thoracic region. A SIPU device was placed next to the PMHS to prevent it from falling onto the ground and producing further injury. The impact was performed by a pneumatic ram. On the ram was a load cell that could measure the force of the ram on the body throughout the duration of the impact. Throughout the setup before the test, and after the

test, camera still photographs were taken, and during the test, a handheld camera also recorded the impact. Figure 5.3 shows the test setup.

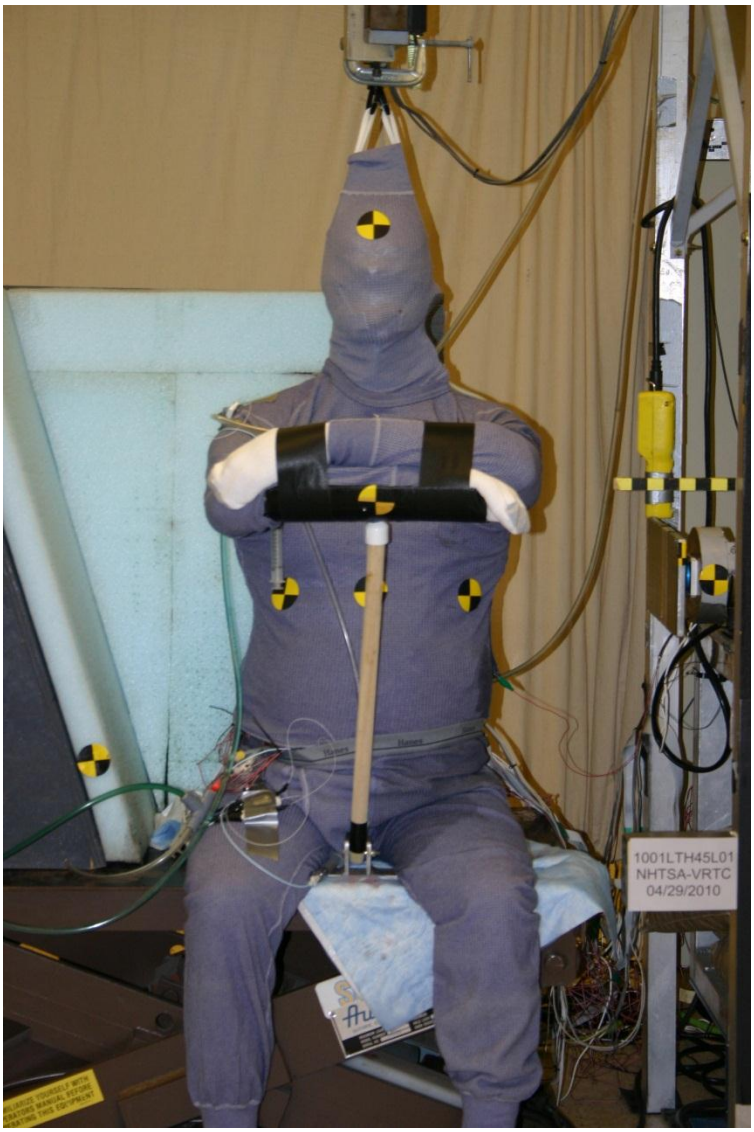

Figure 4.2: Pre-Test Setup for 1001LTH45L01

After impact, an autopsy was performed, paying attention to rib fractures, the ligementum arteriosum, the heart, blood vessels, the lungs, the thoracic vertebrae, and the thoracic muscles. Figure 4.3 shows the thoracic cage during the autopsy. Appendix A has a sample autopsy report [8].

Figure 4.3: Autopsy of Rib Cage after Test 1001LTH45L01. There were no fractures.

4.2 Human Rib Strain Gage Procedures:

For each of the 14 thoracic impact tests, different amount of strain gages were applied to different ribs. The strain gage matrix below demonstrates what type of strain gage preparation, strain gage, and which ribs were used in each test.

Table 4.1: Strain Gage Application Matrix					
Test Number	Model Gage	Taping	Silicone	Incision	Ribs with Gages
801	N/A	N/A	N/A	N/A	N/A
802	Gen Purpose	none	none	1 long	L5-L10; R5-R10
803	Gen Purpose	none	none	1 long	L5-L10; R5-R10
804	Gen Purpose	none	none	1 long	L5-L10; R5-R10
901	Gen Purpose	taped	none	1 per rib	L3-L10; R3-R10
902	Gen Purpose	taped	none	1 per rib	L3-L10; R3-R10
903	Gen Purpose	taped	none	1 per rib	L3-L10; R3-R10
904	Gen Purpose	taped	none	1 per rib	L3-L10; R3-R10
905	Gen Purpose	taped	none	1 per rib	L3-L10; R3-R10
906	Gen Purpose	taped	none	1 per rib	L3-L10; R3-R10
1001	Gen Purpose	taped	yes	1 per rib	L3-L10; R3-R10
1002	Gen Purpose	taped	yes	1 per rib	L3-L10 ant and post
1003	Gen Purpose	taped	yes	1 per rib	L3-L10 ant and post
1101	Gen Purpose without exposed wire	none	none	1 per rib	L3-L10 lat and obl; R3-R10 lat and obl

In general every strain gage was placed on ribs the same way. First, the strain gage had to be tested and prepared. Vishay General Purpose Strain Gages Item Code 3037385 were used for every test, and a strengthened model of the same item was used during the last test. First, silicon was placed on the back of the strain gage, where the leads attached, to ensure the leads would stay connected to the gage. Next, a piece of labeling tape was placed about 6 inches from the end of the wire that was used for connection to the data acquisition system. After this was completed, the wires were separated towards that same end so they could be more easily plugged into the data acquisition system. Next, the exposed leads of the gage were secured with electrical tape so that the exposed wire would not fail. This involved placing a strip of tape on each side of the gage extending from the head of the strain gage, along the leads and to the wiring. This tape was then cut down in width. After this, another piece of tape was wrapped around the point of connection between the leads and the wiring. Next the resistance was tested throughout the

separate wires to make sure that there was not a short between any electrical connections. After this was done, a catalyst was applied to the surface of the strain gage that would be attached to the rib. Figure 4.4 demonstrates a prepared strain gage.

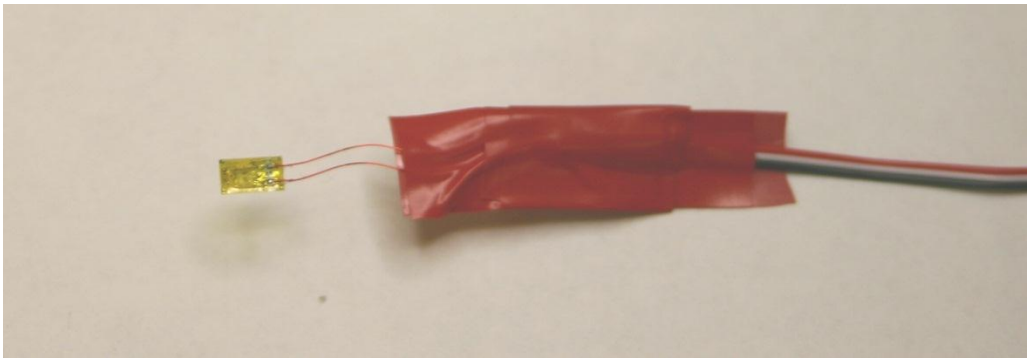

Figure 4.4: Prepared Strain Gage for test 1001LTH45L01

Next the strain gages were attached to the ribs. Slits were cut to expose ribs 3-10. Whether or not both sides were used is found in the Table 5.1. Data on how many strain gages were placed on each rib can also be found in this matrix. Slits of approximately 20 cm in length were cut. Special precaution was made not to cut through intercostal muscles so that the internal anatomy of the thoracic cage was not compromised. After incisions were made to expose a lateral or oblique portion of the rib, each exposed rib was cleaned and scraped where the strain gage would be placed. Some steps above were omitted in some tests. Refer to Table 5.1 to determine if steps were omitted in any given test. Gages were placed either lateral or oblique because impacts were made on the lateral or oblique side of the thorax, and the strain gages were placed where the impact would not happen so that the impacting face would not damage the strain gage. Once each rib was exposed, a finger of a latex glove was placed over the normal personal protective gloves on a member of the lab's finger. The rib was then rubbed with

anhydrous diethyl ether to ensure a dry surface was present for the rib. The person next placed glue on the strain gage and on the finger and glued the gage to the rib. Pressure was applied to the gage for three minutes. All gages were placed on in the same direction, so the wiring would all extend from the subject in the same direction. After all gages were placed on the ribs, the incisions were sutured closed. Figure 4.5 shows gages being placed onto the ribs. The gages were again tested for resistance in case any gages had failed while placing them on the ribs. The wires from the gages were bundled with one another and were sutured to the subject so that the gages would not easily be pulled off the ribs. After the subject was positioned, the wires from the gages were connected to the data acquisition system.

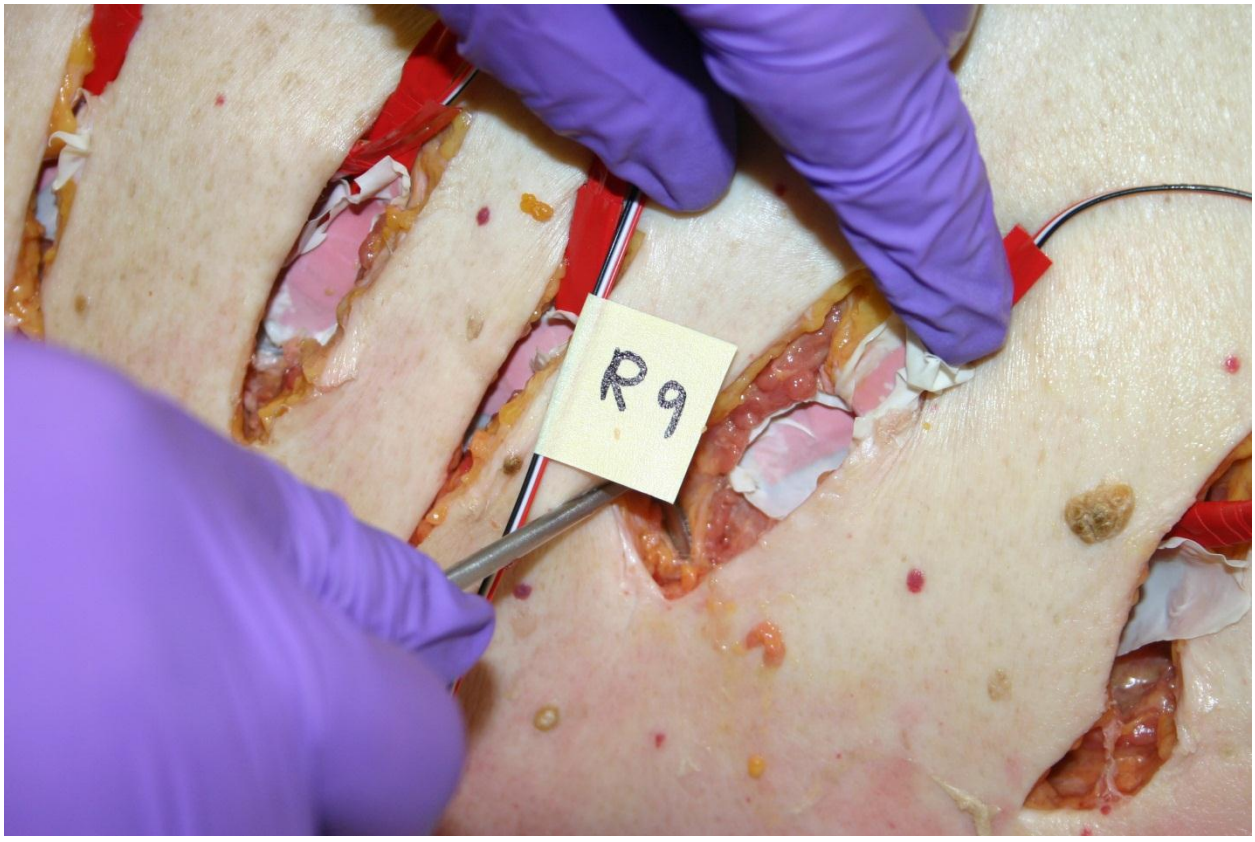

Figure 4.5: Gages Being Applied to Ribs

4.3 Ex vivo Tests

Four human ribs were tested *ex vivo* in a pendulum fracture test with a custom pendulum fixture. First, the human ribs were removed from a PMHS and were cleaned off completely so that there was no flesh left on the bones. Throughout the entire process, the ribs were kept moist with a saline solution so that they would not dry out and lose their material properties. The ribs were potted so that they could be secured in the rib fixture. After the ribs were cleaned and potted, the strain gages were prepared and cleaned. The strain gages were prepared in the same way that they were prepared for the thoracic impact tests. They were then glued onto the rib. Four gages were placed on each rib. Two were placed on the cutaneous surface at 30% and 70% of the rib, and two were placed on the plural surface, also at 30% and 70% of the length of the rib. All wires were placed in the same direction. The gloves covering the strain gages were trimmed so that the gages could be seen. After the gages were placed on the ribs, the rib was placed into the fixture and was impacted. The pendulum acted to compress the rib until it fractured. High speed cameras were set up to record the fracture event. The test setup can be seen in Figure 4.6. After the rib was impacted, measurements and observations from the rib fracture were recorded. This process was repeated with all four ribs. The rib after fracture can be seen in Figure 4.7. Appendix B has a sample data sheet from the *ex vivo* testing.

Figure 4.6: Pendulum Test Setup

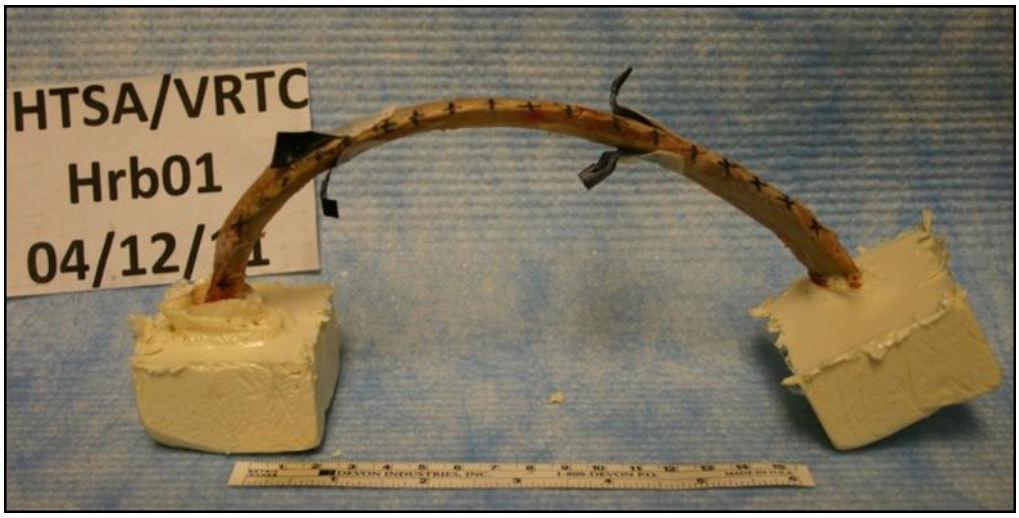

Figure 4.7: Rib After Testing

4.4 Data Analysis

First a subjective blind study was conducted in order to become more familiar with the strain gage signals. Without knowing the results of the autopsy, all signals were viewed. First, failed signals had to be picked out because they did not give reliable data. Failed signals showed no strain throughout the trial, did not return to a magnitude of strain near 0 after the impact, or strain results that showed no set pattern of strain. After this was performed, all signals that did not appear to have failed were analyzed. All signals from the test were analyzed together, because without scaling the signals together, relative magnitudes of strain could not be noted. The first thirteen thoracic impact tests were part of the blind study. Predicted time of fracture, which is defined as the time that correlates to the maximum strain in the subject, was recorded.

Every signal that was analyzed was measured for several characteristics. The decline in strain after the maximum was looked as a sign of fracture instead of the buildup of strain because the definition of a fracture is the release of strain. Strain could either be placed on the rib relatively slowly or quickly, but the rib could still fracture. The definition of the decline in strain after the maximum is the section of the strain gage chart from maximum to the first local minimum. The first measurement that was taken from all tests was the maximum strain. Other measurements that were taken include the maximum magnitude of strain rate after the fracture, the regression slope of the strain rate after the fracture, the time range of the decline in strain after the fracture, and the strain range between the maximum and the first local minimum after the maximum strain. Absolute values were taken for all values because the sign of the strain depended on whether the surface was being extended or compressed, and for the *ex vivo* tests, the

different surfaces of the bone had different signs. All signals were processed using Microsoft Office Excel 2010. Figure 4.8 shows an example plot.

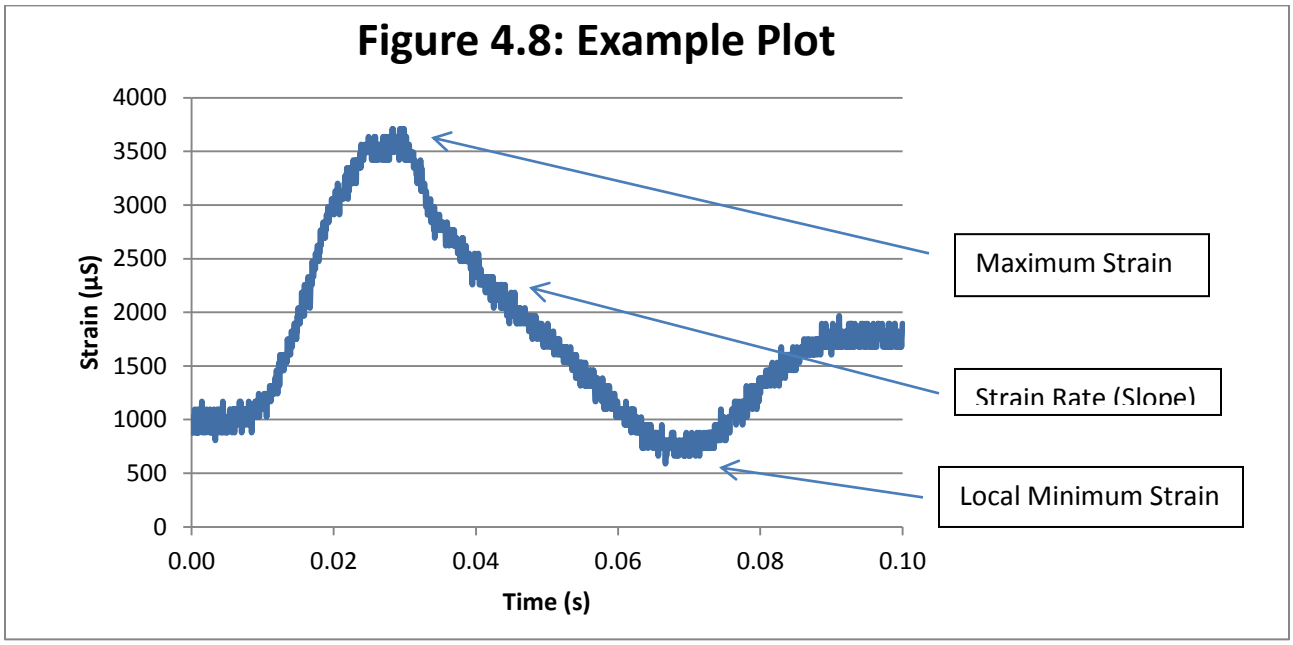

Chapter 5: Results

This section discusses the various data that were analyzed throughout this study. The analysis includes the 13 original thoracic impact tests, the four *ex vivo* trials, and the most recent thoracic impact test with different strain gages.

5.1: 13 Thorax Tests Strain Gage Results

Strain signals were observed for all tests. Four of the 13 tests were excluded from this study. Test 0801 was excluded from the study because no strain data was recorded. Test 0901 was excluded because the signals were clipped before reaching maximum strain. Tests 0905 and 0906 were excluded due to signal noise that made it difficult to determine a peak strain. This study only used non-censored strain results so that results could be applied to future tests before censoring out noise in the data.

Figures 5.1-5.9 show the strain signals from all gages that did not fail. Failed strain gages were removed, and they were determined by signals that did not change in magnitude throughout the test, had major fluctuations throughout the impact, or did not return to zero after the impact. Tests 1002 and 1003 had two strain gages applied to each rib, one was on the anterior side of the thorax and the other was on the posterior side of the thorax. Also, the first rib fracture fail time estimate for each rib that fractured and had a functioning strain gage is listed in Table 6.1. The fracture time estimate is the first maximum point before a major drop off in strain.

Only the time for the first failure is given because the gage could have been detached from the section of the rib that had the second fracture. For 1003, the times of the fractures are taken from the anterior gages only, because they had the larger, better defined signals. Table 5.1 lists the predicted times of fractures for the fractured ribs with good data traces.

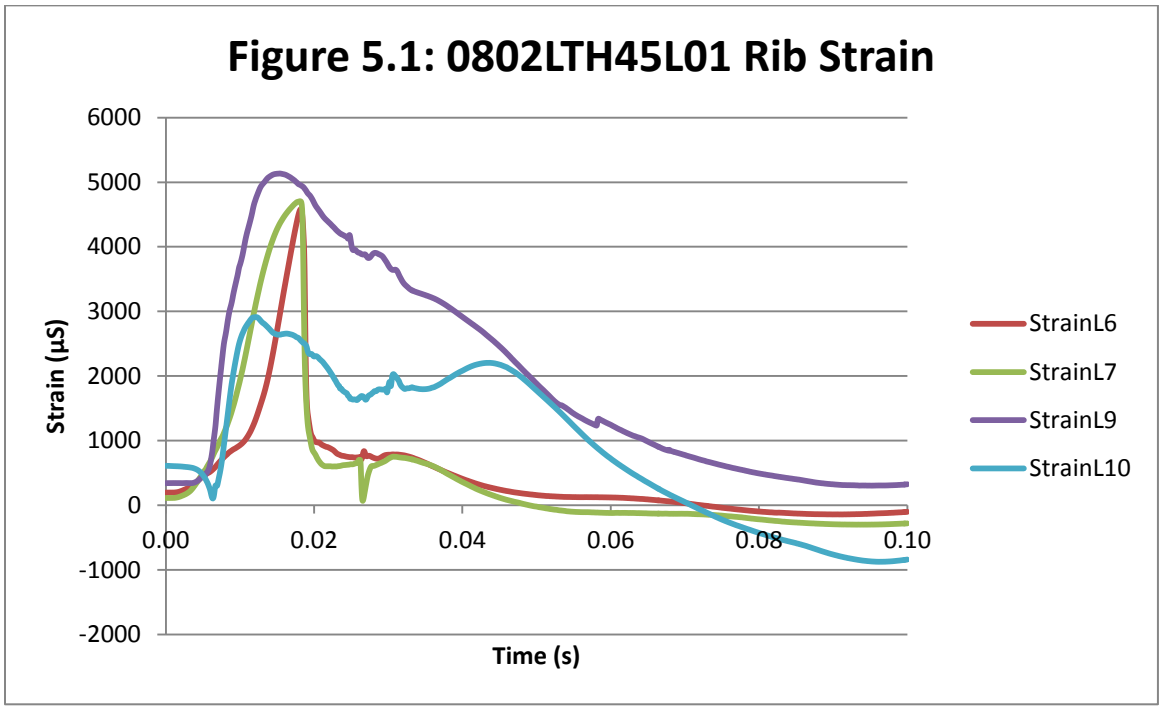

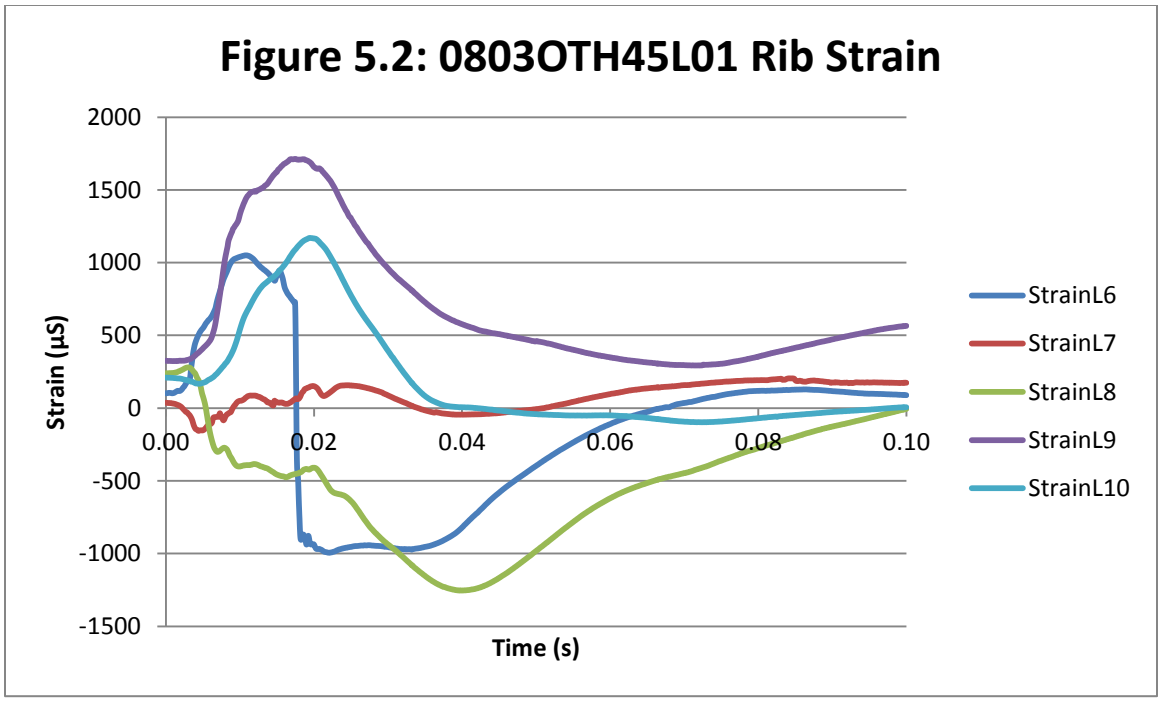
Figure 5.2: 0803OTH45L01 Rib Strain
2000
1500
1000
500
0
-500
-1000
-1500
Strain (µS)
0.00
0.02
0.04
0.06
0.08
0.10
Time (s)
StrainL6
StrainL7
StrainL8
StrainL9
StrainL10

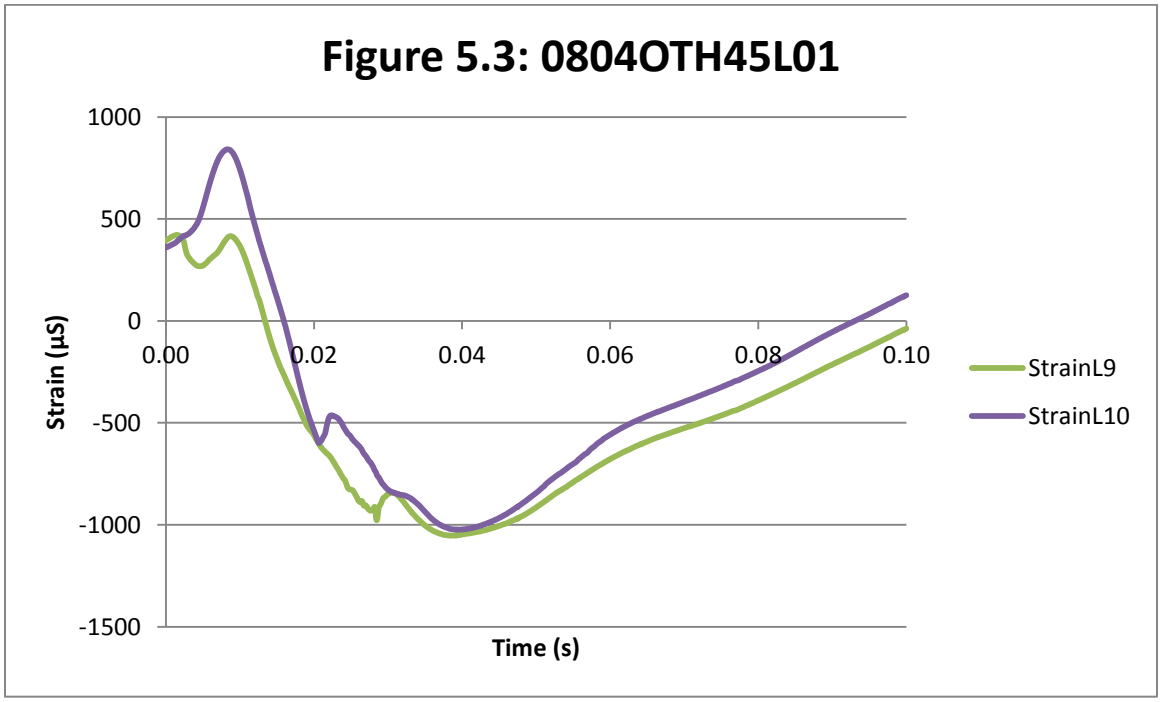
Figure 5.3: 0804OTH45L01
1000
500
0
-500
-1000
-1500
Strain (µS)
0.00
0.02
0.04
0.06
0.08
0.10
Time (s)
StrainL9
StrainL10

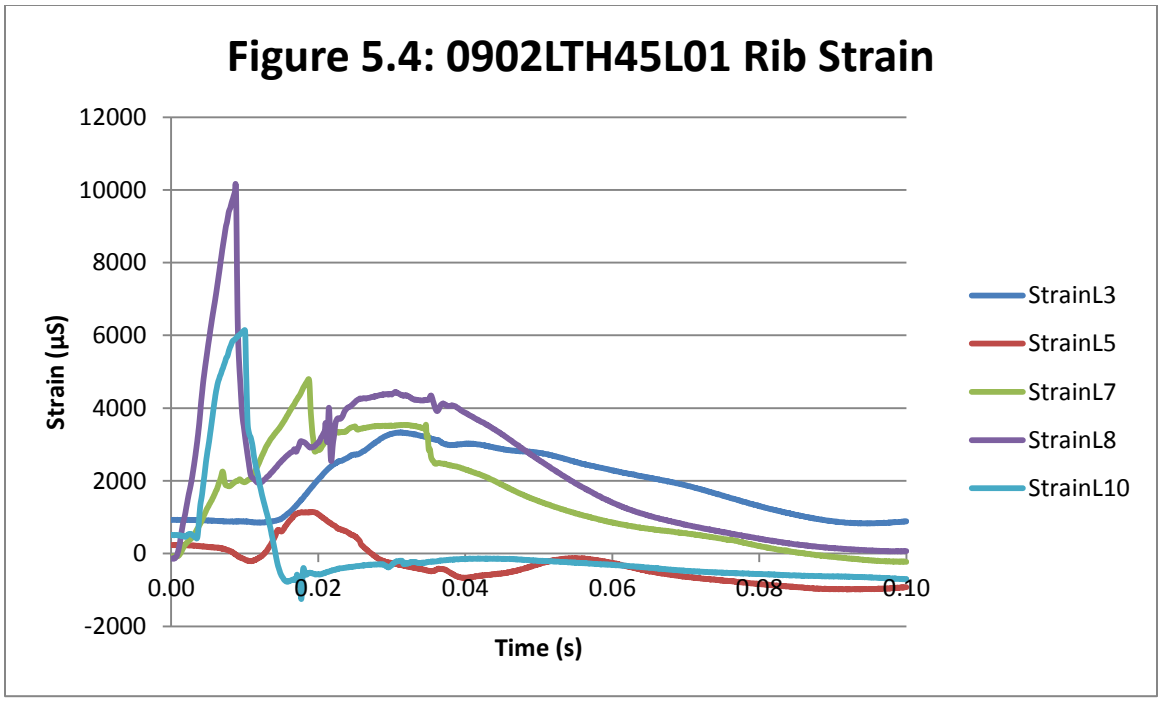
Figure 5.4: 0902LTH45L01 Rib Strain
12000
10000
8000
6000
4000
2000
0
-2000
Strain (µS)
0.00
0.02
0.04
0.06
0.08
0.10
Time (s)
StrainL3
StrainL5
StrainL7
StrainL8
StrainL10

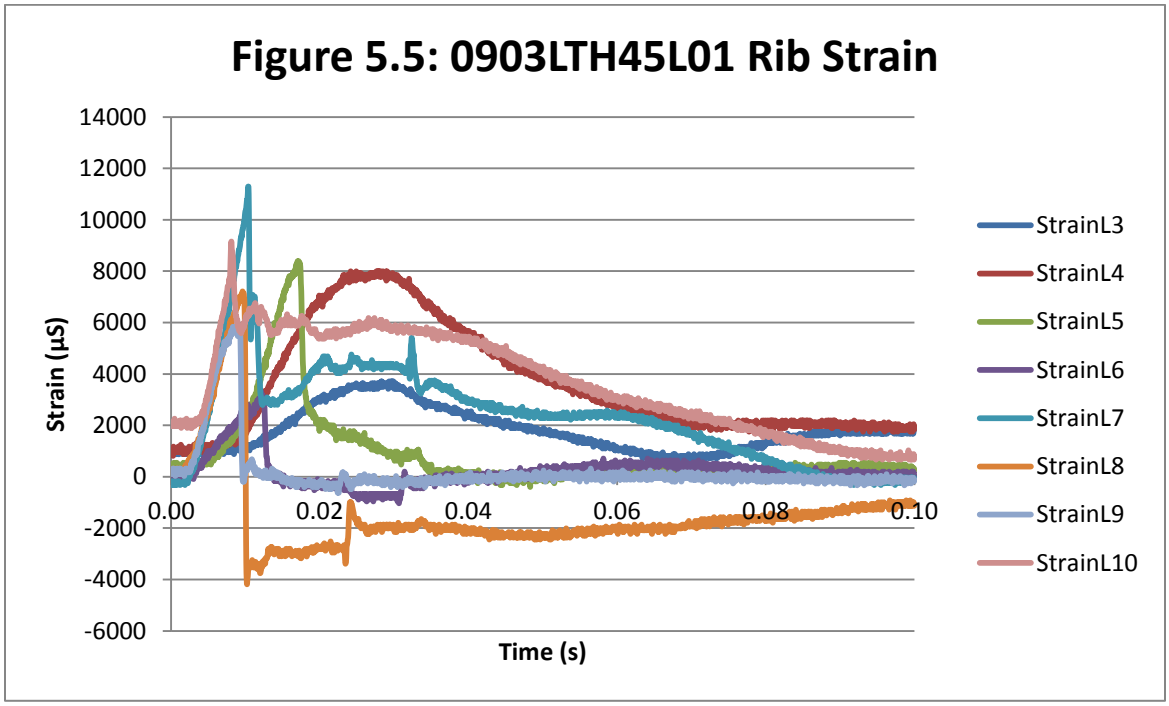
Figure 5.5: 0903LTH45L01 Rib Strain
14000
12000
10000
8000
6000
4000
2000
0
-2000
-4000
-6000
Strain (µS)
0.00
0.02
0.04
0.06
0.08
0.10
Time (s)
StrainL3
StrainL4
StrainL5
StrainL6
StrainL7
StrainL8
StrainL9
StrainL10

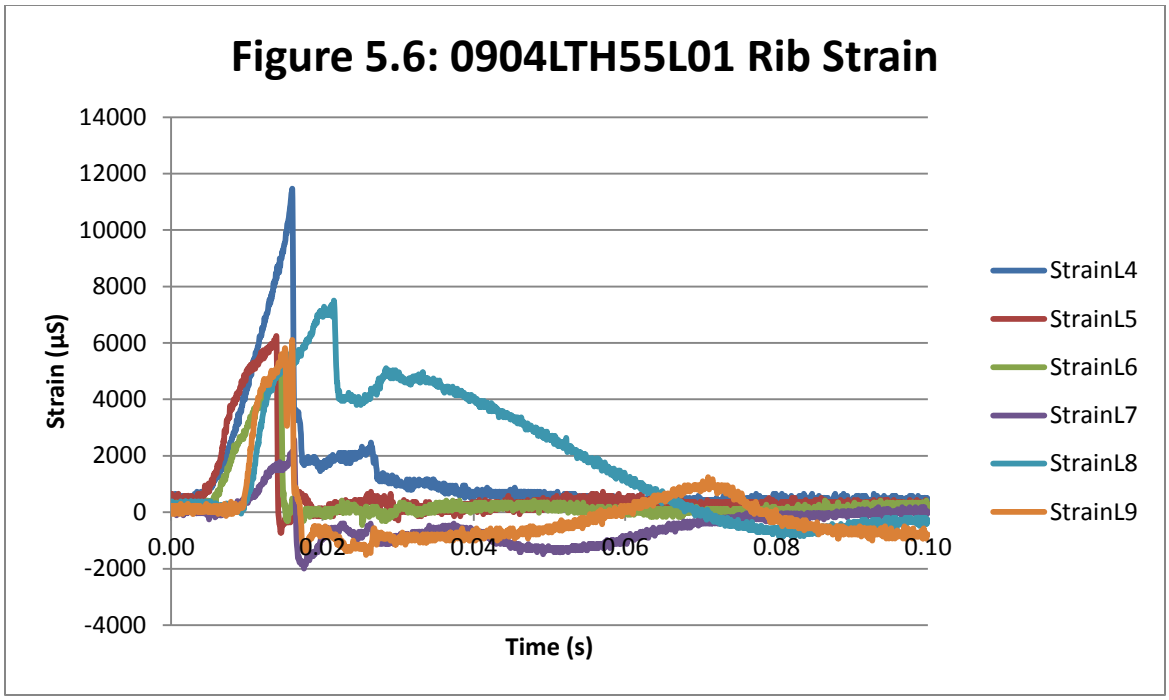
Figure 5.6: 0904LTH55L01 Rib Strain
14000
12000
10000
8000
6000
4000
2000
0
-2000
-4000
Strain (µS)
0.00
0.02
0.04
0.06
0.08
0.10
Time (s)
StrainL4
StrainL5
StrainL6
StrainL7
StrainL8
StrainL9

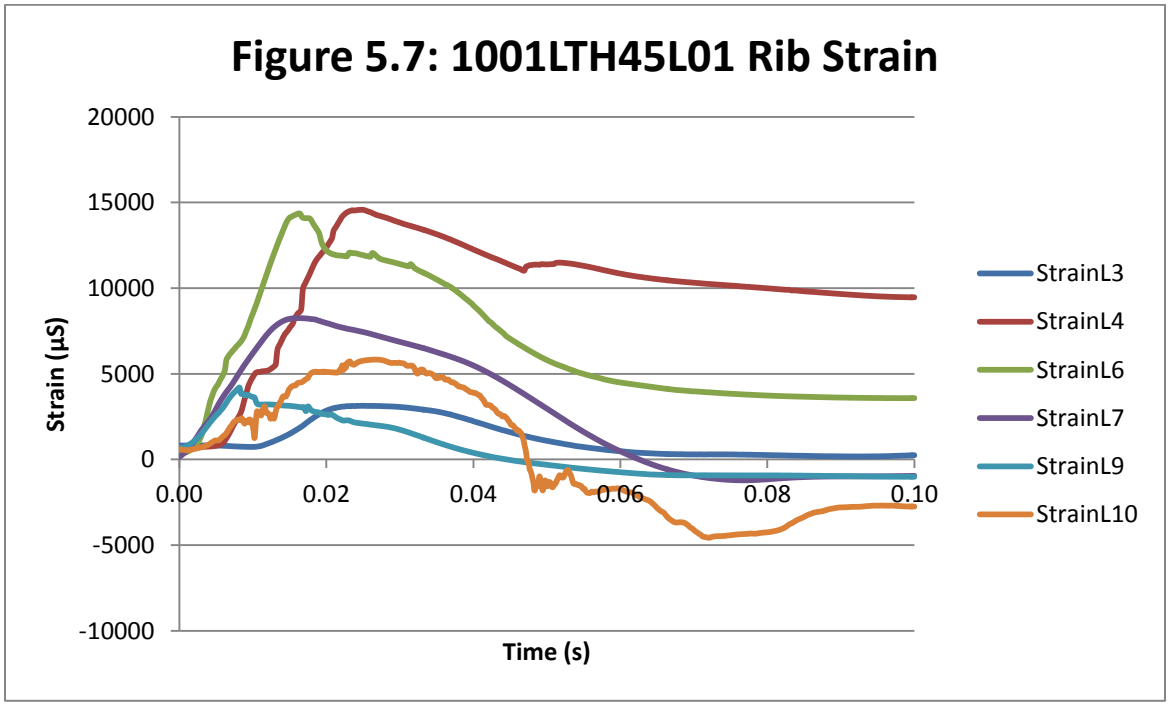
Figure 5.7: 1001LTH45L01 Rib Strain
20000
15000
10000
5000
0
-5000
-10000
Strain (µS)
0.00
0.02
0.04
0.06
0.08
0.10
Time (s)
StrainL3
StrainL4
StrainL6
StrainL7
StrainL9
StrainL10

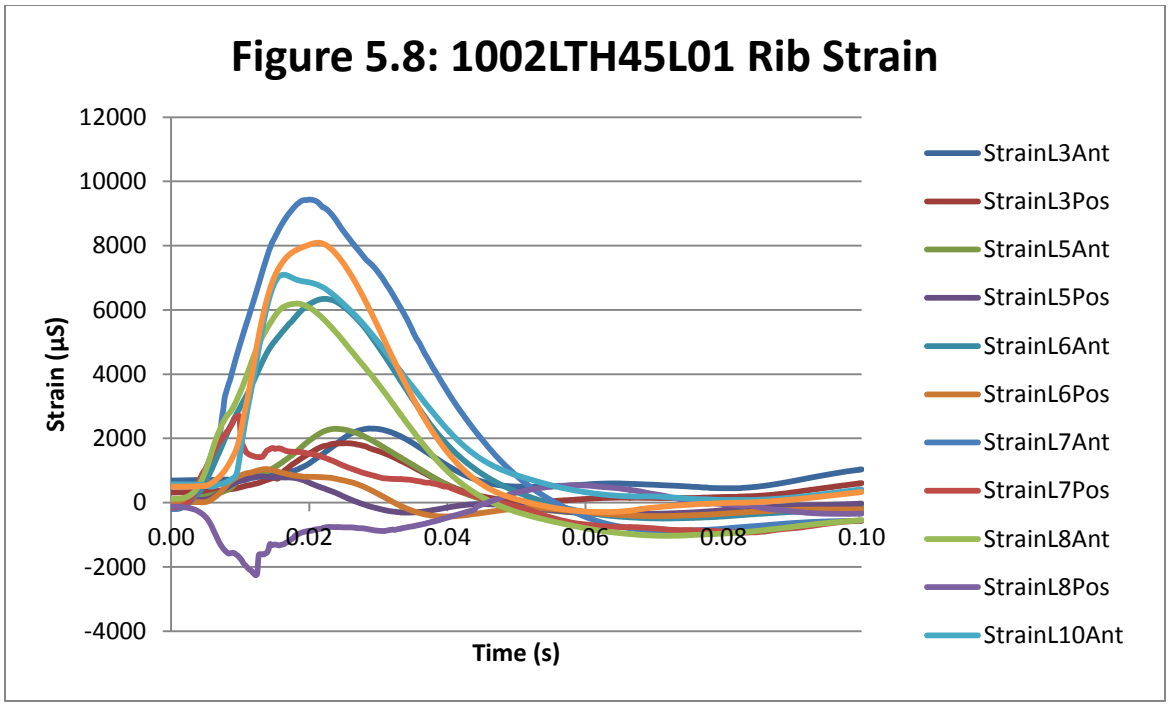
Figure 5.8: 1002LTH45L01 Rib Strain
12000
10000
8000
6000
4000
2000
0
-2000
-4000
Strain (µS)
0.00
0.02
0.04
0.06
0.08
0.10
Time (s)
StrainL3Ant
StrainL3Pos
StrainL5Ant
StrainL5Pos
StrainL6Ant
StrainL6Pos
StrainL7Ant
StrainL7Pos
StrainL8Ant
StrainL8Pos
StrainL10Ant

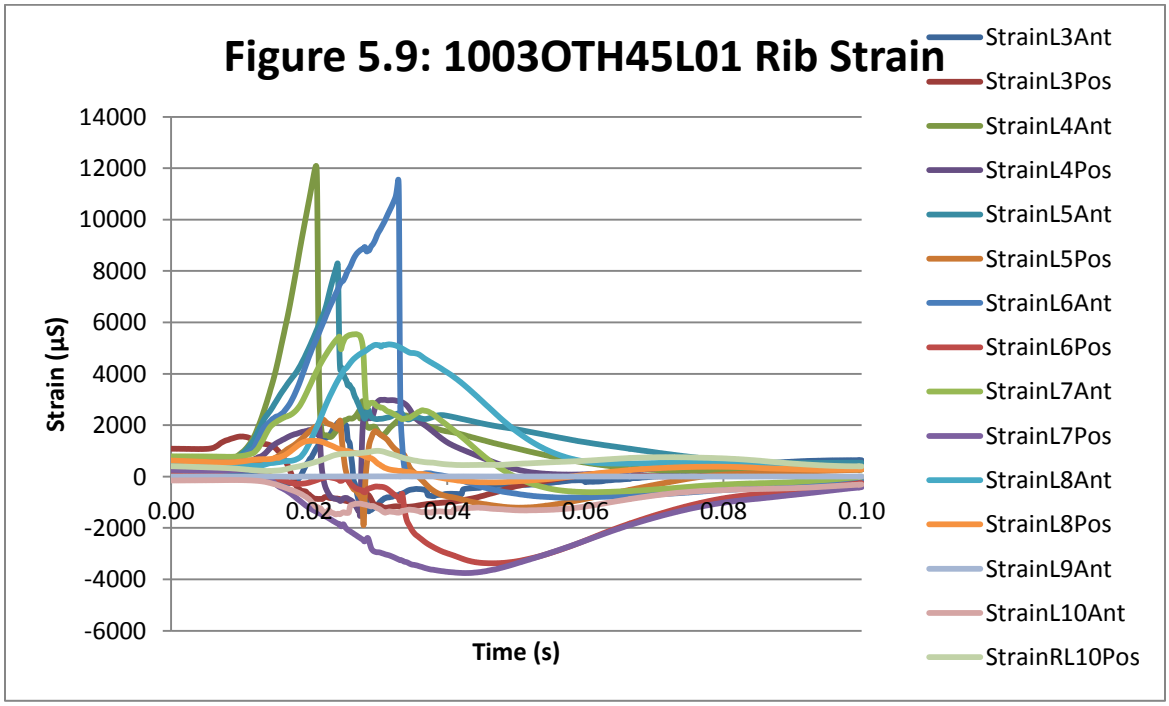
Figure 5.9: 1003OTH45L01 Rib Strain
14000
12000
10000
8000
6000
4000
2000
0
-2000
-4000
-6000
Strain (µS)
0.00
0.02
0.04
0.06
0.08
0.10
Time (s)
StrainL3Ant
StrainL3Pos
StrainL4Ant
StrainL4Pos
StrainL5Ant
StrainL5Pos
StrainL6Ant
StrainL6Pos
StrainL7Ant
StrainL7Pos
StrainL8Ant
StrainL8Pos
StrainL9Ant
StrainL10Ant
StrainRL10Pos

Table 5.1: Time of Fracture Estimates	
Rib	Time (s)
0803L6	0.0107
0902L5	0.019
0902L7	0.01875
0902L8	0.00875
0902L10	0.0105
0903L4	0.0249
0903L5	0.01715
0903L6	0.0121
0903L7	0.01035
0903L8	0.0096
0903L9	0.00845
0903L10	0.0081
0904L4	0.016
0904L5	0.0139
0904L6	0.01435
0904L7	0.01625
0904L9	0.016
1003L3	0.02425
1003L4	0.021
1003L5	0.0241
1003L6	0.0329
1003L7	0.0268

Without the autopsy report, it was difficult to determine the signals that showed a fracture and the signals that did not show a fracture. For example, when looking at individual signals, the trend in the strain appeared to have the characteristics of a signal that denoted a fracture, but when the signal was compared to other signals, it no longer did, because of difference in magnitude of strain. Figure 5.10 below demonstrates this issue.

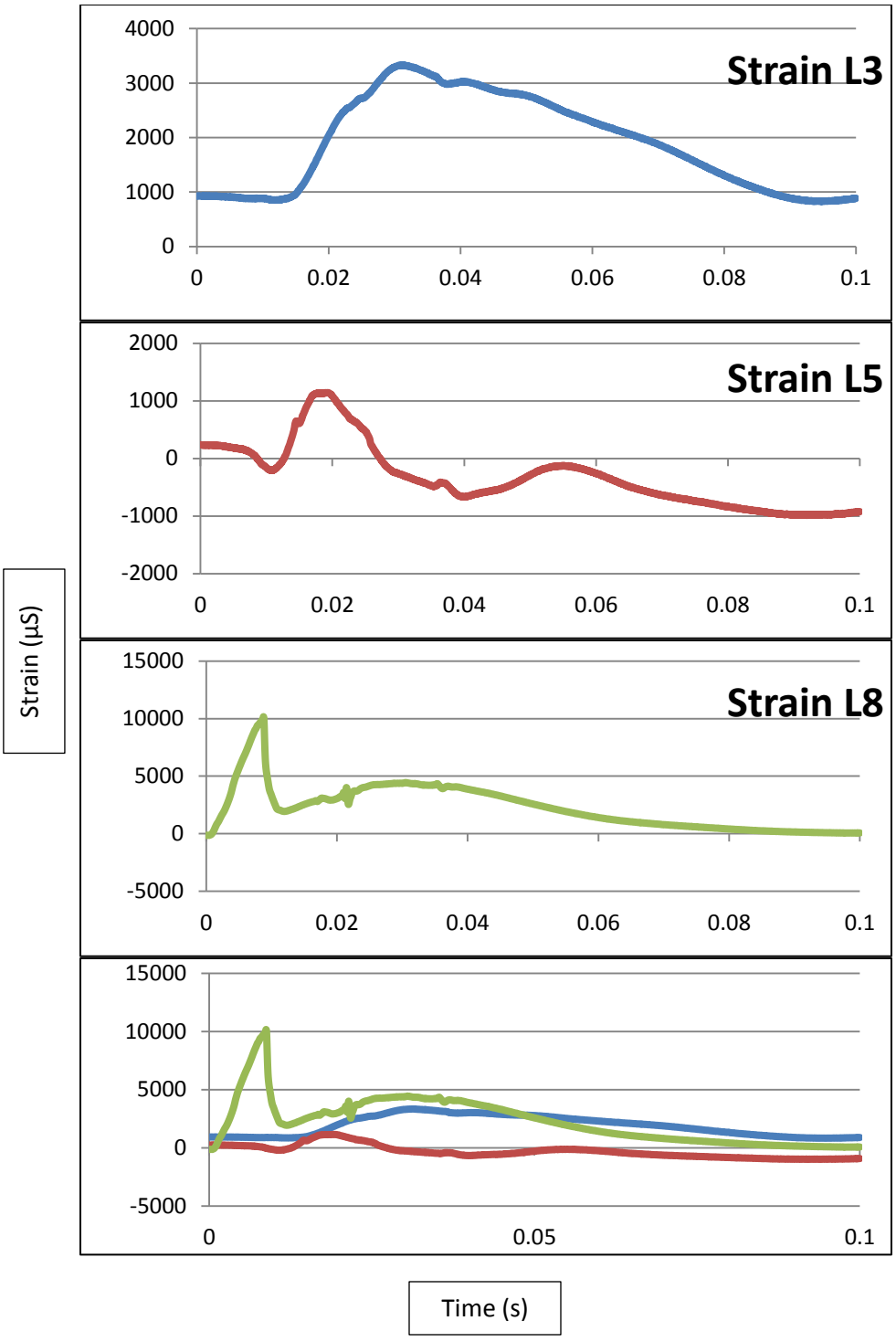

Figure 5.10: Unpredictable Data

Three of the individual signals in Figure 5.10 were taken from the same test. This demonstrates the difficulty of qualitatively predicting fractures. Rib L3 was correctly predicted to have no fracture. Rib L5 was incorrectly predicted to have fractured. Rib 8 was correctly predicted to have fractured. The graph at the bottom shows all three signals, all from the same test, on the same scale. The shapes of the curves look different on different time scales, making it difficult to make a good prediction qualitatively.

5.2 Quantitative Analysis of Thorax Data

First, eight random strain gage signals that were selected correctly were isolated. Several statistics were recorded from the signals. Maximum Strain, Strain Range, the maximum magnitude of slope between any two data points, and a 20% to 80% regression curve were recorded. The 20% to 80% regression curve is a linear regression plot of the data 20% of the range from the maximum to local minimum from both the maximum and minimum. Any points that fell within the 20% to 80% of the strain range were included in this regression plot. These 8 gages were selected to be representative of the greater population of correctly guessed fractured ribs. Table 652 below shows the data. All time measurements are in seconds. All strain measurements are in microstrain, and all slope measurements are in microstrain/second.

Table 5.2: Correctly Predicted Fractures									
test	rib	time max	max strain	time min	min strain	strain range	min slope	Regression	R Squared
902	L8	8.75E-03	1.02E+04	1.20E-02	1.94E+03	8.23E+03	-1.89E+07	-4.23E+06	0.9205
902	L10	1.00E-02	6.15E+03	1.59E-02	-7.74E+02	6.92E+03	-9.52E+06	-9.75E+05	0.9774
904	L4	1.60E-02	1.15E+04	1.97E-02	1.45E+03	1.00E+04	-4.64E+07	-4.64E+07	1.0000
904	L5	1.39E-02	6.25E+03	1.46E-02	-7.25E+02	6.97E+03	-3.49E+07	-3.34E+07	0.9994
904	L6	1.44E-02	5.28E+03	1.55E-02	-3.10E+02	5.59E+03	-2.32E+07	-1.87E+07	0.9734
1003	L4ant	2.10E-02	1.21E+04	2.31E-02	1.54E+03	1.06E+04	-3.50E+07	-2.77E+07	0.9833
1003	L5ant	2.41E-02	8.30E+03	2.80E-02	2.25E+03	6.05E+03	-1.72E+07	-1.62E+07	0.9988
1003	L6ant	3.29E-02	1.16E+04	3.61E-02	8.22E+01	1.15E+04	-4.76E+07	-3.40E+07	0.9681
average		1.76E-02	8.91E+03	2.06E-02	6.82E+02	8.23E+03	-2.91E+07	-2.27E+07	0.9776
minimum		8.75E-03	5.28E+03	1.20E-02	-7.74E+02	5.59E+03	-4.76E+07	-4.64E+07	0.9205
maximum		3.29E-02	1.21E+04	3.61E-02	2.25E+03	1.15E+04	-9.52E+06	-9.75E+05	1.0000

The same was done for signals that were correctly predicted as non-fractured rib signals.

Table 5.3 demonstrates this.

Table 5.3: Correctly Predicted Non-Fractures									
test	rib	time max	max strain	time min	min strain	strain range	min slope	Regression	R Squared
902	L3	3.13E-02	3.33E+03	9.46E-02	8.27E+02	2.51E+03	-4.06E+05	-4.59E+04	0.9952
1001	L6	1.63E-02	1.44E+04	9.81E-02	3.58E+03	1.08E+04	-1.80E+06	-2.31E+05	0.9305
1001	L7	1.61E-02	8.25E+03	7.68E-02	-1.22E+03	9.47E+03	-3.14E+05	-2.45E+05	0.9935
1001	L9	8.15E-03	4.20E+03	9.95E-02	-1.01E+03	5.21E+03	-2.57E+06	-1.09E+05	0.9918
1002	L5ant	2.37E-02	2.30E+03	6.90E-02	-4.02E+02	2.70E+03	-1.80E+05	-1.20E+05	0.9958
1002	L6ant	2.23E-02	6.34E+03	7.12E-02	-4.95E+02	6.84E+03	-3.74E+05	-2.72E+05	0.9866
1002	L7ant	2.01E-02	9.43E+03	7.24E-02	-8.83E+02	1.03E+04	-5.82E+05	-3.42E+05	0.9944
1002	L8ant	1.84E-02	6.20E+03	7.14E-02	-1.03E+03	7.23E+03	-3.44E+05	-2.64E+05	0.9960
average		1.95E-02	6.80E+03	8.16E-02	-8.02E+01	6.88E+03	-8.22E+05	-2.04E+05	0.9855
min value		8.15E-03	2.30E+03	6.90E-02	-1.22E+03	2.51E+03	-2.57E+06	-3.42E+05	0.9305
max value		3.13E-02	1.44E+04	9.95E-02	3.58E+03	1.08E+04	-1.80E+05	-4.59E+04	0.9960

The data for both the fractured ribs and non-fractured ribs both have a large range in most of the categories compared. It was determined that any possible criteria to use should not overlap between the fractured and non-fractured signals. Because of this, the maximum strain was first eliminated as a choice for determining whether or not a fracture occurred since the maximum value of 14400 microstrain for the non-fractured ribs was greater than 5280 microstrain for the minimum of the fractured signals. After this, strain range was also eliminated because again, the maximum value of 10800 microstrain for the non-fractured ribs was larger than the minimum value of 5590 microstrain for the fractured ribs. Next, the maximum magnitude of slope between any two points in the data was looked at. This produced a separated range, but some of the data had noise in it. Because of this noise, the data would need to be censored to use this maximum magnitude of slope between any two points. This is because a signal with noise might have slopes between two points that are not representative of the greater trend. That left the regression slope to be utilized. Separation exists between the correctly predicted fracture and correctly predicted non-fracture range.

This data was next applied to incorrectly predicted strain signals to determine whether or not the quantitative analysis could do what the qualitative analysis could not do. The cutoff used to determine the range for the regression slope was a magnitude of 659,000 microstrain per second, which is the average of the maximum magnitude for the non-fractures and the minimum magnitude for the fractured signal regression plots. This was compared to the incorrectly fractured signals. The autopsies revealed that 0902L5, 0903L4, and 1003L3Ant all had fractured, and 0802L6 and 0904L8 had not fractured.

Table 5.4: Incorrectly Predicted Signals									
test	rib	time max	max strain	time min	min strain	strain range	min slope	Regression	R Squared
902	L5	1.93E-02	1.14E+03	3.54E-02	-4.89E+02	1.63E+03	-6.39E+05	-1.45E+05	0.9531
1003	L3Ant	2.43E-02	2.11E+03	2.72E-02	-8.97E+02	3.01E+03	-3.28E+06	-1.94E+06	0.9470
802	L6	1.82E-02	4.58E+03	2.64E-02	7.07E+02	3.88E+03	-9.49E+06	-6.42E+06	0.9565
903	L4	2.89E-02	7.99E+03	7.78E-02	1.75E+03	6.24E+03	-1.02E+07	-1.58E+05	0.9722
904	L8	2.15E-02	7.50E+03	2.25E-02	3.94E+03	3.56E+03	-1.02E+07	-8.28E+06	0.9845

This cutoff correctly predicts 1003L3Ant and incorrectly predicts the other signals. Because of this, it was determined that a strict cutoff point could not be used to determine whether or not a rib fractured. The data from this test, along with data from the *ex vivo* tests and most recent thorax test were combined to create a logistic binary regression plot in Figure 5.20 that could give a prediction of whether or not a rib fractured based on the strain rate after the peak.

5.3: Ex vivo Testing

For the four ribs tested *ex vivo*, results are graphed below in Figures 5.11-5.14. In test HRB02, gage PSG1 failed. In test HRB03, gage PSG2 failed, and in test HRB04, gage CSG1 failed. The vibration in the strain gage signals were caused by the vibrations of the table in the pendulum test. The gages labeled CSG1 and CSG2 are on the cutaneous side of the rib, and the gages labeled PSG1 and PSG2 are on the pleural side of the rib.

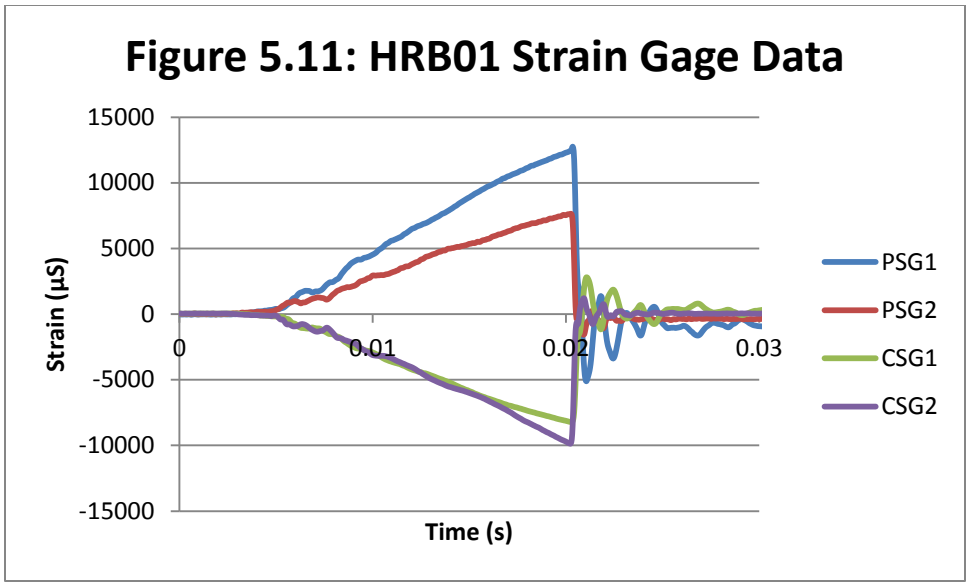
Figure 5.11: HRB01 Strain Gage Data
15000
10000
5000
0
-5000
-10000
-15000
Strain (µS)
0
0.01
0.02
0.03
Time (s)
PSG1
PSG2
CSG1
CSG2

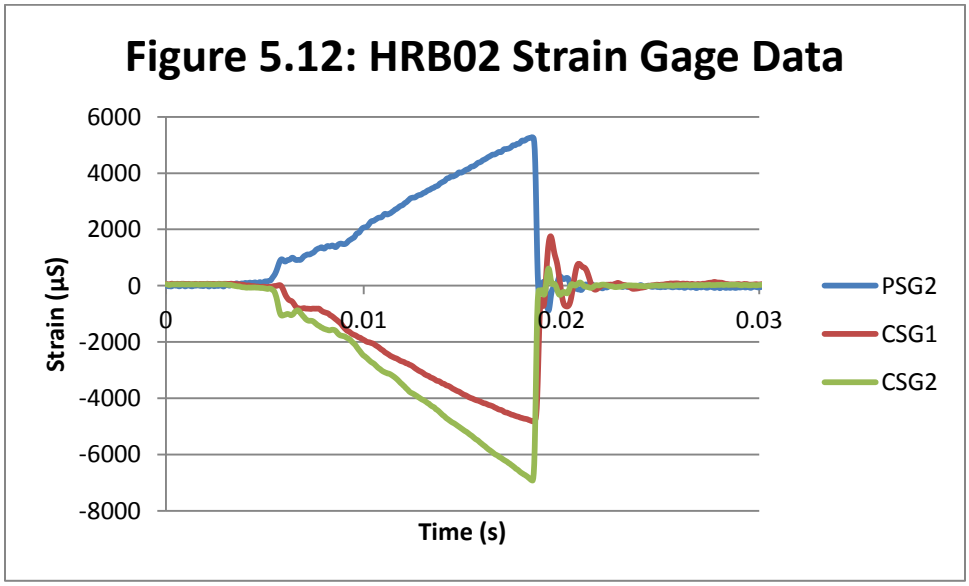
Figure 5.12: HRB02 Strain Gage Data
6000
4000
2000
0
-2000
-4000
-6000
-8000
Strain (µS)
0
0.01
0.02
0.03
Time (s)
PSG2
CSG1
CSG2

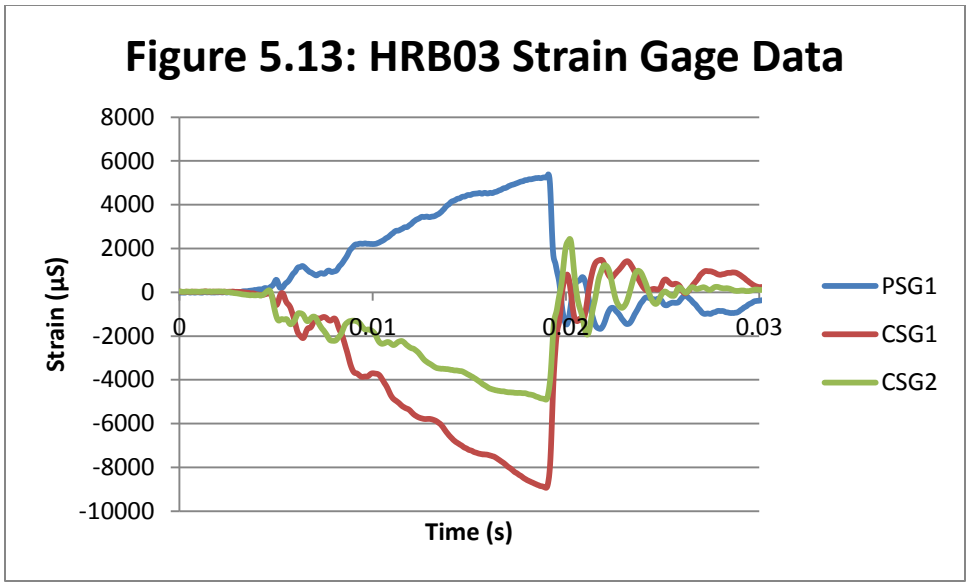

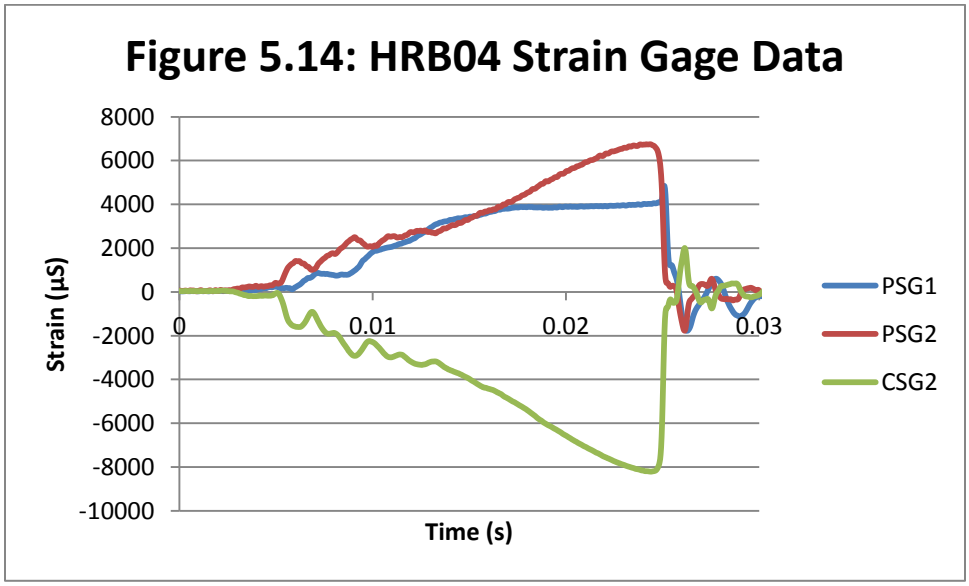

In this testing, the pleural side of the rib underwent tension, which is noted by the positive strain values, while the cutaneous gages underwent compression. This is opposite the human thorax testing, where the only gages placed on were cutaneous. In the thorax testing, all the strain was positive. This demonstrates that the mechanism of fracture was different for the *ex vivo* tests and the thoracic impacts.

The statistical analysis was repeated for the human rib *ex vivo* testing. It can be seen below in Table 5.5.

Table 5.5: Ex Vivo Testing Data

Test	gage	time max strain	max strain	time min strain	min strain	strain range	Min Slope	Regression	R Squared
HRB01	PSG1	2.04E-02	1.28E+04	2.11E-02	5.11E+03	1.79E+04	6.11E+07	2.65E+07	0.9547
HRB01	PSG2	2.03E-02	7.65E+03	2.09E-02	1.56E+03	9.21E+03	5.07E+07	1.55E+07	0.8333
HRB01	CSG1	2.03E-02	8.21E+03	2.11E-02	2.79E+03	1.10E+04	3.63E+07	1.56E+07	0.9675
HRB01	CSG2	2.02E-02	9.85E+03	2.09E-02	1.20E+03	1.11E+04	5.55E+07	1.82E+07	0.8732
HRB02	PSG2	1.85E-02	5.27E+03	1.89E-02	2.32E+02	5.51E+03	3.53E+07	1.70E+07	0.9096
HRB02	CSG1	1.86E-02	4.82E+03	1.90E-02	4.84E+02	4.34E+03	2.52E+07	1.16E+07	0.8896
HRB02	CSG2	1.86E-02	6.92E+03	1.89E-02	1.72E+02	6.75E+03	4.10E+07	2.60E+07	0.9608
HRB03	PSG1	1.91E-02	5.38E+03	2.01E-02	1.47E+03	6.85E+03	2.22E+07	7.07E+06	0.9245
HRB03	CSG1	1.90E-02	8.93E+03	2.01E-02	8.12E+02	9.74E+03	2.56E+07	1.04E+07	0.9450
HRB03	CSG2	1.90E-02	4.90E+03	2.02E-02	2.44E+03	7.34E+03	1.59E+07	6.57E+06	0.9738
HRB04	PSG1	2.51E-02	4.84E+03	2.63E-02	1.78E+03	6.61E+03	2.21E+07	4.93E+06	0.9098
HRB04	PSG2	2.44E-02	6.75E+03	2.62E-02	1.77E+03	8.52E+03	2.68E+07	5.62E+06	0.8921
HRB04	CSG2	2.44E-02	8.21E+03	2.54E-02	3.43E+02	7.87E+03	3.66E+07	1.01E+07	0.8450
average		2.06E-02	7.27E+03	2.14E-02	1.55E+03	8.67E+03	3.49E+07	1.35E+07	0.9138
maximum		2.51E-02	1.28E+04	2.63E-02	5.11E+03	1.79E+04	6.11E+07	2.65E+07	0.9738
minimum		1.85E-02	4.82E+03	1.89E-02	1.72E+02	4.34E+03	1.59E+07	4.93E+06	0.8333

Every rib fractured in the *ex vivo* tests, and the gages all show the 20% to 80% regression slope to be well above the cutoff from the thorax testing. Absolute values were taken of all values so averages, minimum, and maximums could be calculated. Also, the distance from the gage to the fracture could be accurately measured during this testing in Table 5.6. Figure 5.15 below demonstrates whether or not there is correlation between regression slope and distance from fracture to gage. This figure shows that there is no measurable correlation between distance and strain rate.

Table 5.6: Gage to Fracture Distance Data			
test	gage	distance from fx (mm)	Regression
HRB01	PSG1	45	26455788
HRB01	PSG2	40	15546689
HRB01	CSG1	60	15646661
HRB01	CSG2	35	18160830
HRB02	PSG2	25	17017667
HRB02	CSG1	65	11618271
HRB02	CSG2	25	25985980
HRB03	PSG1	50	7067702
HRB03	CSG1	50	10403236
HRB03	CSG2	45	6565224
HRB04	PSG1	60	4928817
HRB04	PSG2	25	5618427
HRB04	CSG2	25	10087426

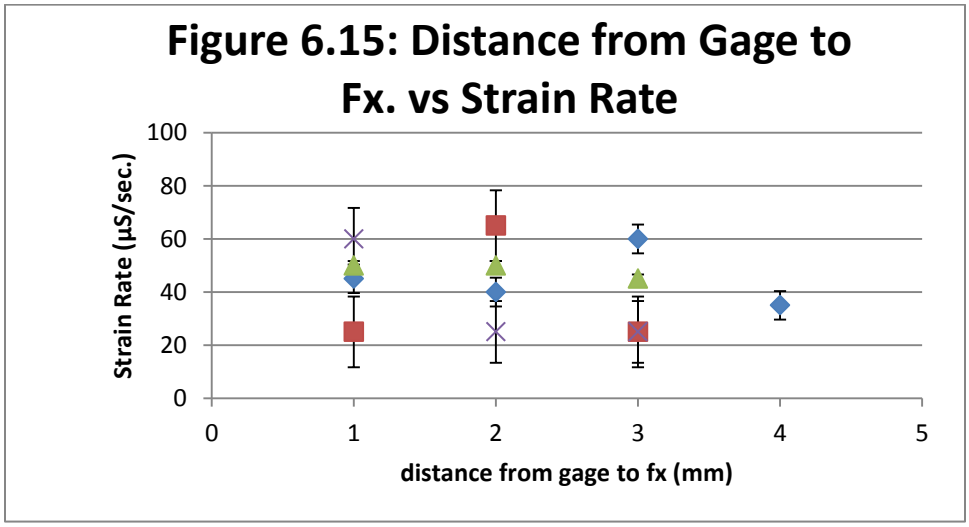

5.4 Recent Thorax Test

The recent thoracic impact was different from earlier tests, because it contained four impacts on the same subject. Four impacts were performed because the strain gages showed no sign of fracture at all. Figures 5.17-5.20 show the strain data from these tests.

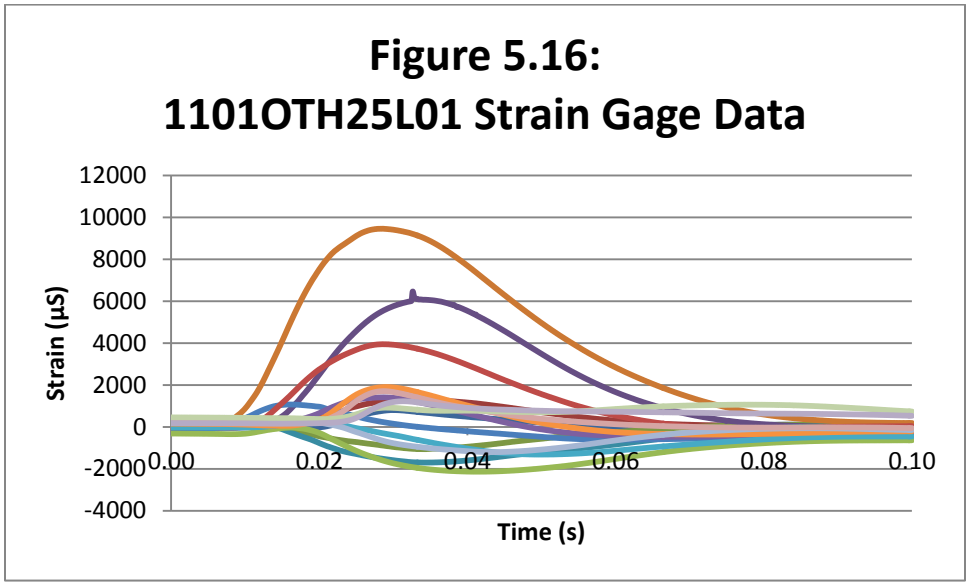

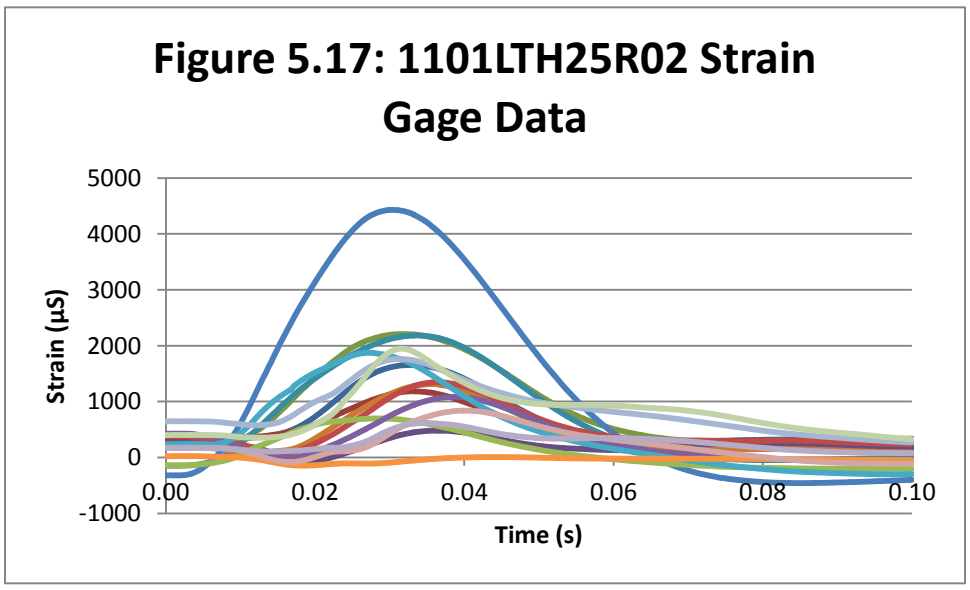

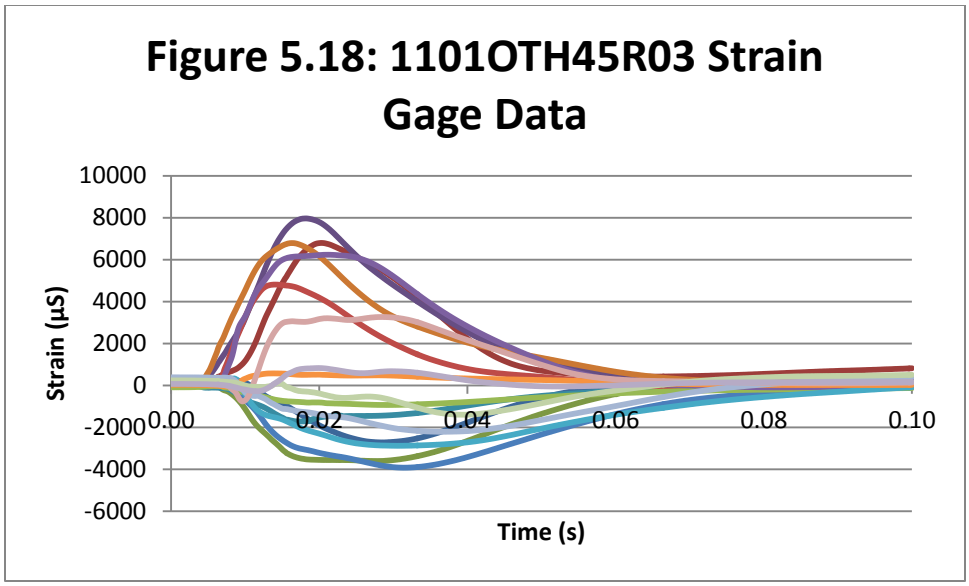

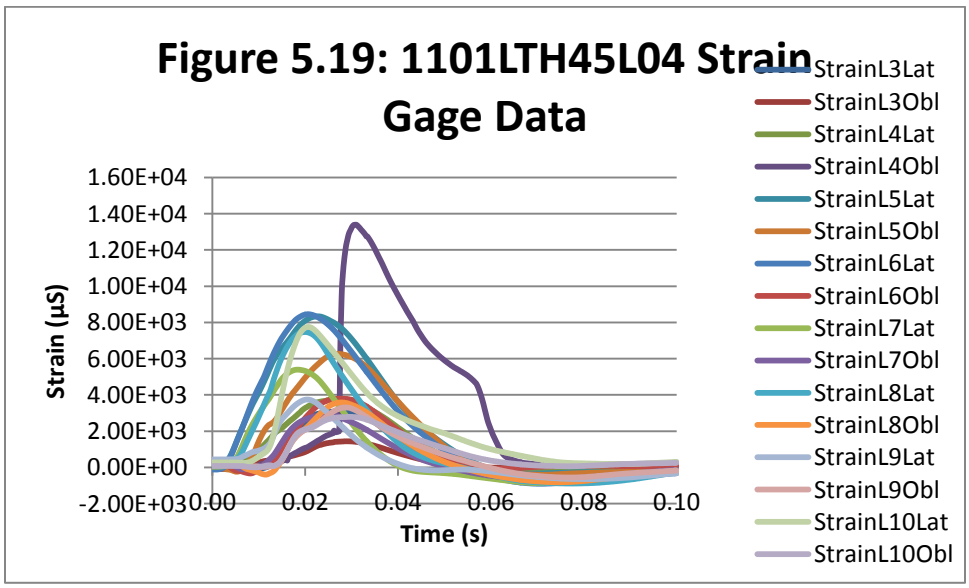

From each of the four tests, the two gages that showed the maximum strain were taken and used for the binary logistic regression plot along with the original thoracic tests and the *ex vivo* testing.

Table 6.7: 1101 Test Strain Gage Data									
Test	gage	time max	max strain	time min	min strain	strain range	min slope	Regression	R Squared
1101OTH25L01	L4Obl	3.26E-02	6.56E+03	9.31E-02	1.46E+00	6.56E+03	-1.65E+06	-1.93E+05	0.9949
1101OTH25L01	L5Obl	2.86E-02	9.46E+03	9.92E-02	1.84E+02	-9.27E+03	-3.50E+05	-2.22E+05	0.9891
1101LTH25R02	L5Lat	3.36E-03	2.18E+03	8.06E-02	-4.84E+01	2.23E+03	-1.48E+05	-8.62E+04	0.9950
1101LTH25R02	R6Lat	3.03E-02	4.43E+03	8.55E-02	-4.60E+02	4.89E+03	-2.64E+05	-1.62E+05	0.9965
1101LTH45R03	R4Obl	1.82E-02	7.97E+03	7.66E-02	6.22E+01	7.90E+03	-4.26E+05	-2.24E+05	0.9930
1101LTH45R03	R5Obl	1.64E-02	6.79E+03	7.97E-02	1.71E+02	6.62E+03	-4.08E+05	-1.45E+05	0.9391
1101OTH45L04	L4Obl	3.10E-02	1.34E+04	8.08E-02	6.07E+01	1.33E+04	-1.08E+06	-3.00E+05	0.9655
1101OTH45L04	L6Lat	2.05E-02	8.46E+03	7.09E-02	-9.05E+02	9.36E+03	-3.96E+05	-2.80E+05	0.9891
average		2.26E-02	7.40E+03	8.33E-02	-1.17E+02	5.20E+03	-5.91E+05	-2.02E+05	0.982775
maximum		3.26E-02	1.34E+04	9.92E-02	1.84E+02	1.33E+04	-1.48E+05	-8.62E+04	0.9965
minimum		3.36E-03	2.18E+03	7.09E-02	-9.05E+02	-9.27E+03	-1.65E+06	-3.00E+05	0.9391

This graphical data demonstrates that the regression slopes fall into the range of the non-fractured rib data from the original thorax testing.

5.5 Binary Logistic Regression

After collecting all 42 data points, a binary logistic regression plot was created as a predictor for when a rib fractured or not based on the slope of the strain gage signal after the maximum point. The p-value for this test is 0.000 and the Goodman-Kruskel Gamma value is 0.82. A p-value of 0 is representative of a good fit. A gamma value closer to 1 shows perfect

predictive ability of the regression chart to predict future results[1].

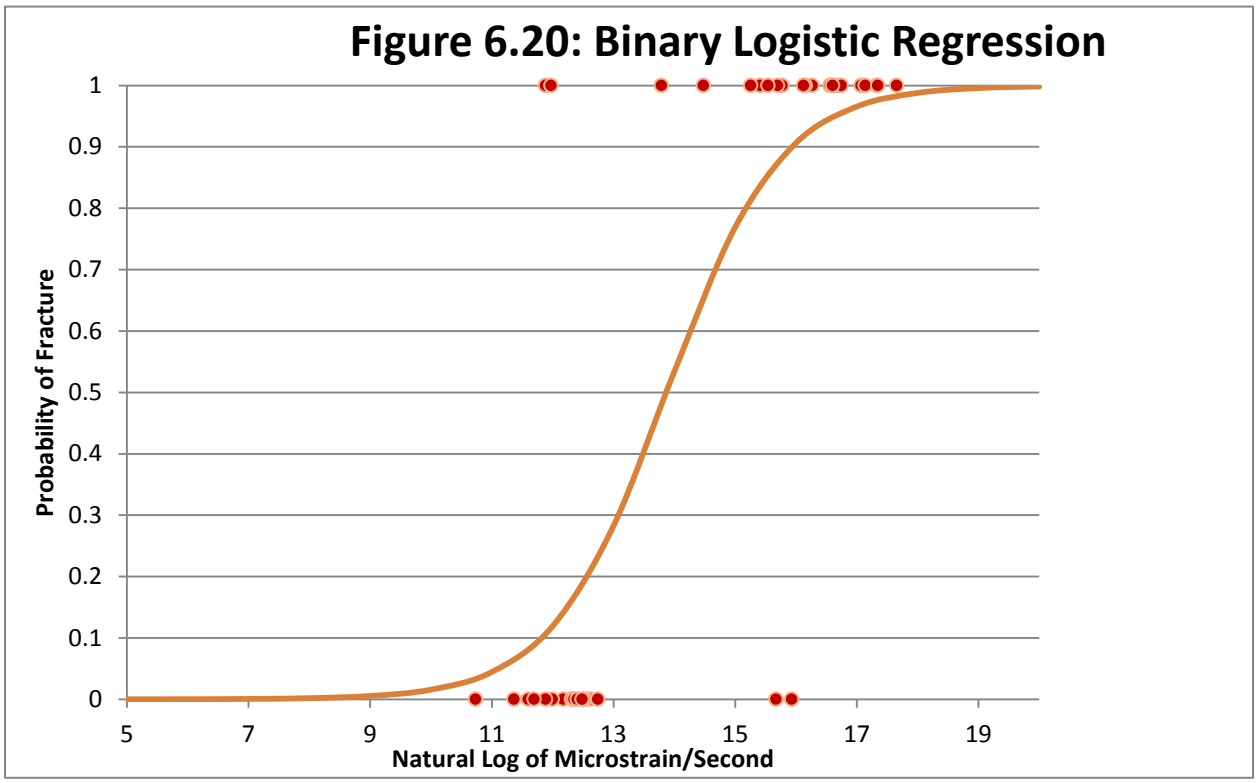

The results of the binary logistic regression plot show that there is a 50% chance of the rib fracturing if the natural log of the slope of the microstrain vs. time graph is 13.9. This correlates to a strain rate of 1,060,000 microstrain per second.

Chapter 6: Discussion, Improvements, and Future Work

6.1 Discussion

The original thirteen thoracic tests demonstrated many things about understanding how to predict whether or not a rib fractured in a thoracic impact. First, it is worth noting what the strain gage testing revealed about the limitations of strain gages in impact testing. It appears that the reason strain gages failed was because of failure of the leads or connection between the leads, wiring, and gage surface. It does not appear that the gages failed because of actual damage to the gage face. If this were the case, it would be noted that gage failures would be consistent throughout all tests even after the wiring and leads were supported. For the first three tests 61% of gages showed accurate signals. For the last three tests, 78% of gages showed accurate signals. Throughout the testing, ribs were strengthened with more and more techniques including taping the leads and placing silicone to adhere the leads to the gage better.

For the signal statistics, the strain rate after the maximum point was used for multiple reasons. The first reason is that the definition of a fracture is the breaking of a bone after a force was applied to it. The strain rate leading to the maximum point showed the force being applied to the bone. No matter how quickly or slowly the force was applied, at a certain point, the rib would fracture due to the increased strain on the bone. The shapes of strain before the maximum for the fractured ribs varied greatly. The slope of the strain graph after the maximum was used because the fracture event releases the strain in the bone causing the rapid decrease of strain.

Duma et al did not use the strain rate after the fracture because of the possibility of it failing at the maximum. Multiple autopsy reports from that study showed the fracture occurring at the gage, which could contribute to the reasoning behind that theory [3,4]. However, there is no reason to justify that the gage would fail after the maximum otherwise unless the impact damages the gage. Maximum strain and strain range were not used as measureable results, because there was less correlation between them and the fracture outcome.

The *ex vivo* testing revealed multiple things about the test setup. First, the direction of the strain was worth noting. During the *ex vivo* testing, the cutaneous side of the rib was in compression, while the pleural side of the gage was in tension. This is the opposite of the human thorax testing, but it is because of different mechanisms of fracture. There tended to be a general trend that strain rate was lower the farther away the gage was from the fracture, but there was not enough solid evidence to accurately determine if that is correct or not. The change in strain rate was only significant if one gage was more than 1 cm closer to the fracture than the other. There was also no significance in

Limited insight was given by the 1101 thorax test. Figures 5.17-5.20 show the strain gage signals, but without any fractures to compare the signals to, it is difficult to know how close the ribs came to fracture or how much strain they could handle. Graphically, it does appear that there is a correlation between impact speed and maximum strain on the ribs. The last two tests involved ribs being impacted at higher speeds. However the thorax was impacted in different locations for the various speeds. The tests labeled OTH were obliquely impacted, and the tests labeled LTH were laterally impacted. It is also worth noting that in the lateral impacts, all gages underwent tensile strain only, but during the oblique impacts, some gages underwent compression strain also.

Finally, after all the data was collected and measured, the binary logistic regression plot was created. It can be seen in Figure 5.21 that the regression plot shows that there is a 50% chance of a rib fracture if the strain rate after the maximum is above 1,060,000 microstrain per second, which correlates with a natural log on the graph of 13.9. There is a 10% chance of a rib fracture if the natural log of the strain rate is 11.8, which is a strain rate of 13,600 microstrain per second. This data can be used for future trials, because a program can be created to take the signal and analyze for this piece of data. After a test, the strain rates could be determined, and if they are above a certain level, testing could stop or a CT scan could be performed to determine if a fracture actually occurred before more testing occurred. This will have the limitation of only being able to determine the presence or absence of fractures and not how many fractures occurred, but that can be analyzed during an autopsy after the test.

Strain rate was chosen as a better fit for the binary logistic regression than maximum strain or stain range. Maximum strain rate was an effective measure. It was even more effective than the regression strain rate, but because it excludes any signals with noise, it was not used. Table 6.1 shows all of the p values for the test that all slopes are zero, gamma values, and chi square values for the four measurements tested for the binary logistic regression. Of the five incorrectly predicted signals, the binary logistic regression predicted one of them correctly.

Table 6.1: Binary Logistic Regression Statistics

	Tests that all slopes are zero P-value	Hosmer-Lemeshow Chi-Square P-value	Goodman-Kruskal Gamma value
absolute value of regression	0	0.42	0.83
natural log of absolute value of regression	0	0.24	0.82
absolute value of minimum slope	0	0.93	0.96
maximum strain	0.68	0.25	0.11
strain range	0.28	0.74	0.19

6.2 Improvements

Several improvements could be made to this study. Most of the improvements involve using the new, more robust strain gages. With the older signals, even taped, several gages failed, leaving bad signals. There is always the fear that other signals failed in less noticeable ways, and these failed signals could have been used in the data. In order to get a truly representative binary logistic regression, all data must be accurate to the strain on the rib. Because the only way to know if a gage failed is to visually examine the signal, it is possible that a failed gage could have appeared to have not failed. Throughout all testing, more effort must be made into recording the distance along the rib from every gage to every fracture, the condition the gage is in during the autopsy report, taking more photographs during autopsy to determine whether the gage was along the correct axis or if there was an offset. Thoracic testing impact speed and conditions were not looked into in this thesis, but they could be correlated with fractures so that they could be utilized to help predict presence of fracture. During the *ex vivo* tests, the table must be secured better to the ground so that vibrations do not interrupt the strain gage signal noticeably. This could affect the regression slope of each signal.

6.3 Future Work

Future work for quantitatively studying strain gage signals to determine whether or not a fracture has occurred will involve completing more strain gage tests with the new strain gage models to determine the difference it makes and if the new strain gages have the same limitations

in predicting fractures, because no rib with the robust strain gage has fractured at The Ohio State University. The only test they were involved in had no fractures through four impacts. After this is completed, the data points taken from the gages should be compared to the binary logistic regression to determine whether or not they fit with the regression. If they do not, a new binary logistic regression should be created with multiple points from the new testing. More *ex vivo* tests should be completed with the robust strain gages so that the results can be compared to the results from the *ex vivo* tests with the strain gages with exposed wires to determine if the sensitivity differences make a significant difference in the results.

Chapter 7: Conclusions

- The most effective quantitative measure for predicting whether or not a fracture occurred without observing autopsy is the magnitude of the strain rate after the fracture event.
- There is a 10% chance of a fracture if the magnitude of the strain rate is 13,600 microstrain per second after the maximum strain magnitude.
- There is a 50% chance of fracture if the magnitude of the strain rate is 1,060,000 microstrain per second.
- New, robust strain gages do not fail nearly as often as the older model that was used in the earlier 13 thoracic tests.
- These robust strain gages need more testing to determine if they agree with the binary logistic regression of this study and to determine if they have any problems in testing where fractures occurred.
- The *ex vivo* tests and the thoracic impact tests have different mechanisms of fracture because the cutaneous surfaces of the ribs during the thoracic impact tests undergo tension while the cutaneous surfaces of the ribs during the *ex vivo* tests undergo compression.

References

1. Bolte, J. H., et al. (2004). “Injury and Impact Response of the Shoulder Due to Lateral and Oblique Loading.” Dissertation, The Ohio State University, Columbus 393 p.
2. Borman, J. B., et al. (2006). “Unilateral flail chest is seldom a lethal injury.” Emergency Medicine Journal 23: 903-905
3. Duma, S., J. Stitzel, et al. (2005). “Non-censored rib fracture data from dynamic belt loading tests on the human cadaver thorax.” International Technical Conference on the Enhanced Safety of Vehicles (ESV).
4. Duma, S., et al. (2011). “Rib Fracture Timing in Dynamic Belt Tests With Human Cadavers.” Clinical Anatomy 24: 327-338
5. Gabrielli, F., D. Subit, et al. (2009). "Time-frequency analysis to detect bone fracture in impact biomechanics. Application to the thorax." Medical Engineering & Physics 31: 952-958.
6. Gray, H. (1918). “Anatomy of the Human Body." Bartleby. Web. 23 May 2011. <http://www.bartleby.com/107/>.
7. Human Body. Encyclopædia Britannica Online. Web. 23 May. 2011. <http://www.britannica.com/EBchecked/media/121130/The-human-heart-in-situ>.
8. Long, et al. (2009). “Biomechanical Response of the PMHS Thorax to High Speed Lateral and Oblique Impacts.” Masters Thesis, The Ohio State University, Columbus. 144 p.
9. National Highway Traffic and Safety Administration. (2011). “Early Estimate of Motor Vehicle Fatalities in 2010.” U.S. Department of Transportation, Washington, D.C.

10. Omega Engineering, Inc. (1998). “The Strain Gage.” Transactions: Force-Related Measurements 3: 15-25.

11. Trosseille, X., P. Baudrit, et al. (2008). "Rib cage strain pattern as a function of chest loading configuration." Stapp Car Crash Journal 52: 205-231.

Appendix A: Sample Autopsy Report:

Autopsy Date: 10/28/2010

Autopsy Report

1003OTH45L01

- Diaphragm:
  - No Injury
- Heart & Aortic Arch:
  - No Injury
- Kidney:
  - No Injury
- Liver:
  - No Injury
- Lung:
  - No Injury
- Pancreas:
  - No Injury
- Pericardium:
  - No Injury
- Pleura:
  - No Injury
- Pulmonary Artery:
  - No Injury
- Rib Cage:
  - Fractures (measurements recorded in cm taken from the middle of the sternum and inferior to the sternal notch):
    1. L3 ant: Non-displaced fracture
       - Location at costochondral joint
       - 8 cm inferior & 6.5 cm lateral to the sternum
       - Fracture was located 2 cm lateral to the anterior strain gage
    2. L4 ant: Non-displaced fracture
       - 11 cm inferior & 13 cm lateral to the sternum
       - Fracture was located 2 cm lateral to the anterior strain gage
    3. L4 post: Non-displaced fracture
       - 5 cm inferior & 19.5 cm lateral to the sternum
       - Fracture was located 6 cm posterior to the posterior strain gage
    4. L5 ant: Non-displaced fracture
       - Location at costochondral joint

        - 14.5 cm inferior & 14 cm lateral to the sternum
        - Fracture was located 2 cm lateral to the anterior strain gage
    5. L6 ant: Non-displaced fracture
        - Location at costochondral joint
        - 18.5 cm inferior & 14 cm lateral to the sternum
        - Fracture was located ½ cm medial to the anterior strain gage
    6. L7 ant: Non-displaced fracture
        - Location at costochondral joint
        - 22.5 cm inferior & 15 cm lateral to the sternum
        - Fracture was located 2 cm medial to the anterior strain gage
  - Antemortem Fractures
    1. R10
    2. R11
- Spleen:
  - No Injury

Other Notes:

- Tissue thickness at impact site:
  - Upper ram edge: 3.6 cm
  - Middle of ram: 3.0 cm
  - Lower ram edge: 2.0 cm
- Strain Gage Notes
    - Unless noted, all strain gages were found strongly attached to proper rib
  - Anterior Left Side
    - L10 – Placed partially on musculature and subcutaneous tissue; was still loosely attached to the 10^{th} rib
  - Posterior Left Side
    - L3 – Partially loose upon dissection
  - Right Side
    - No strain gages were placed on the right side of the subject

- Ligamentum Arteriosum:
  - Ligamentum arteriosum was intact at autopsy
- Catheter Location:
  - During autopsy the foley catheters were dissected out to note their location:
    - Left Common Carotid Artery – This foley was in proper position with its balloon approximately 2 cm superior to the arch of the aorta, placing the sensors in the arch.

- Descending Aorta – This foley was in proper position with its balloon at the level of the diaphragm and sensors just inferior to the heart
- Inferior Vena Cava - This foley was located inferiorly at the level of the diaphragm. Unfortunately, the balloon popped, thus we tied off both femoral veins in hope of closing off the inferior venous system of the subject.
- Superior Vena Cava – This foley was in proper position with its balloon superior to the right atrium of the heart.

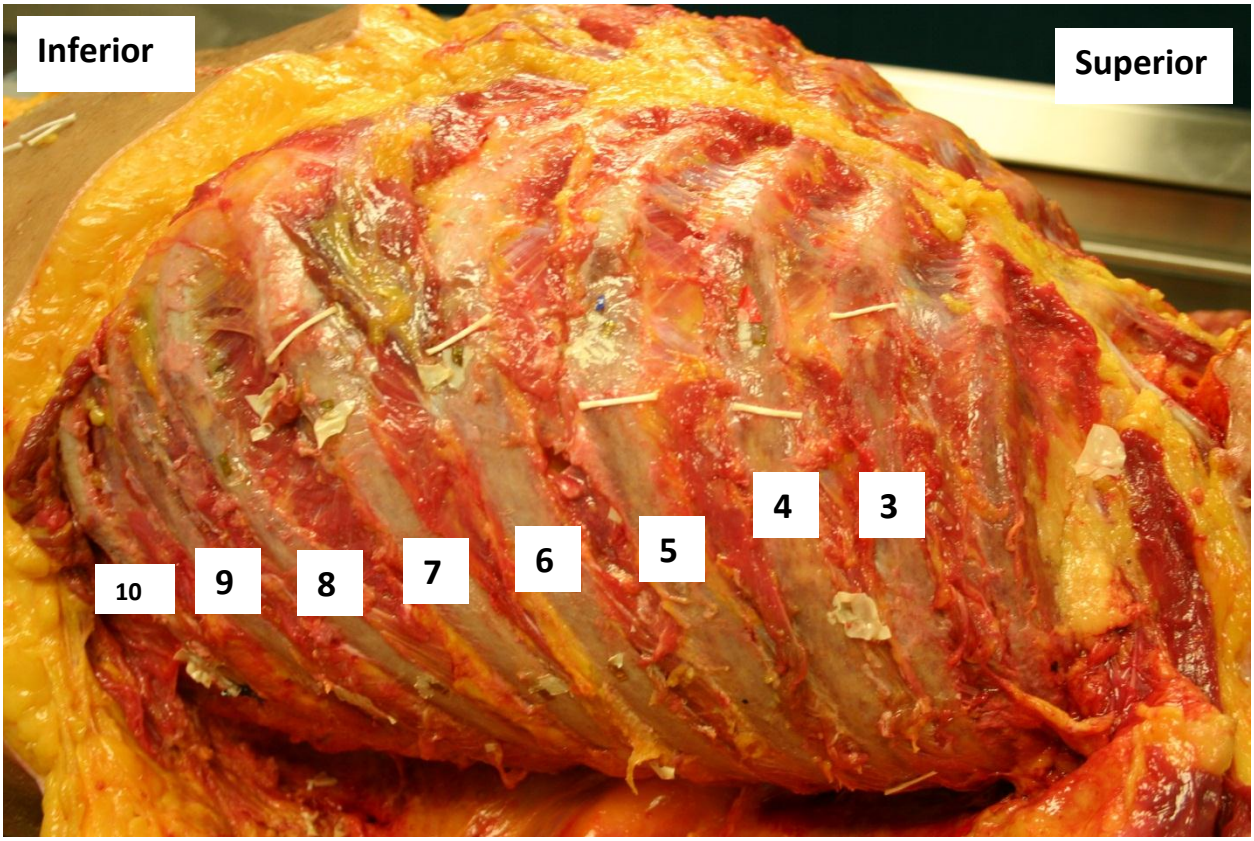

Figure 1: Ribcage of impact (left) side.

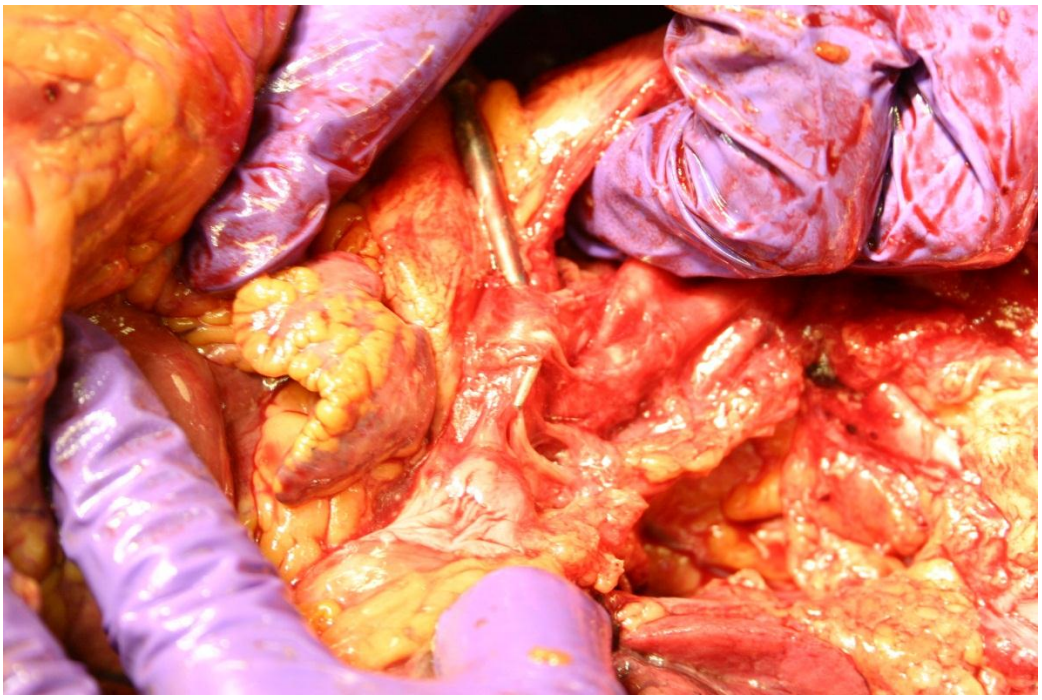

Figure 2: Intact Ligamentum Arteriosum

AIS Code Summary –

- 450230.3 -
  - 6 rib fractures on the left, impact, side of the thorax
  - all fractures were non-displaced, with only one rib (4^{th}) fractured in multiple places
  - stable chest, no pneumothorax

John H. Bolte IV, PhD
Associate Professor, Division of Anatomy
Director – Injury Biomechanics Research Laboratory
The Ohio State University

Appendix B: Sample Data Form from ex vivo test

Potted Rib Measurement Data Sheet

Test/Rib ID: __Hrb01 (5985-R4)_____ Date: ____4/12/11_____

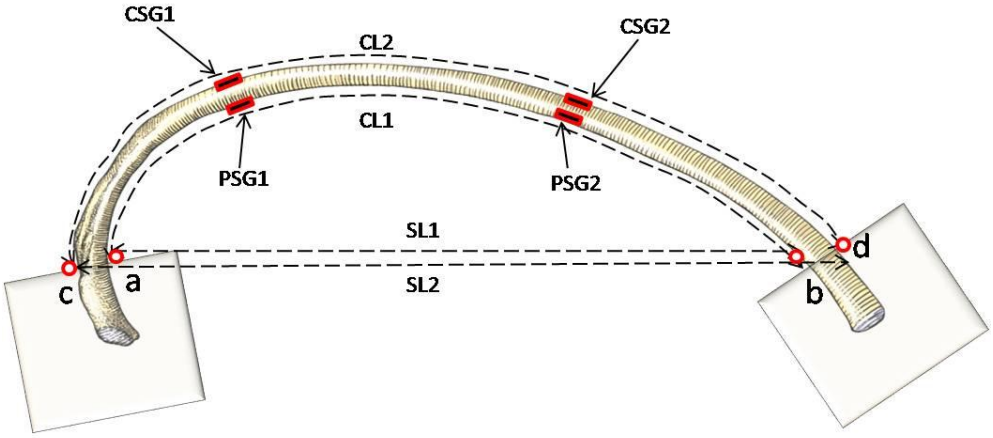

Pre-impact

ID	**Measurement** (mm)	**Description**
Straight Length 1 **(SL1)**:	170	SL1= Linear length from point 'a' to 'b' on ***pleural*** surface
Straight Length 2 **(SL2)**:	190	SL2= Linear length from point 'c' to 'd' on ***cutaneous*** surface
Curve Length 1 **(CL1)**:	215	CL1= Curve length from point 'a' to 'b' on ***pleural*** surface
Curve Length 2 **(CL2)**:	23.5	CL2= Curve length from point 'c' to 'd' on ***cutaneous*** surface
Pleural Strain Gage 1 **(PSG1)**:	65	PSG1= Curve length on ***pleural*** surface to 30% of CL1 from point 'a'
Pleural Strain Gage 2 **(PSG2)**:	150	PSG2= Curve length on ***pleural*** surface to 70% of CL1 from point 'a'
Cutaneous Strain Gage 1 **(CSG1)**:	75	CSG1=Curve length on ***cutaneous*** surface to gage from point 'c' (placed by matching to PSG1)
Cutaneous Strain Gage 2 **(CSG2)**:	165	CSG2=Curve length on ***cutaneous*** surface to gage from point 'c' (placed by matching to PSG2)

Post-impact

ID	**Measurement** (mm)
PSG1	45
PSG2	40
CSG1	60
CSG2	35

*All measurements are from tip of strain gage to end of fracture surface on respective surface. Strain gage tips are all pointed towards the sternal rib end.

Notes:
Transverse fx